The Astrophysical Journal, 1004:46 (26pp), 2026 June 10 https://doi.org/10.3847/1538-4357/ae658c


# Chasing Gamma-Ray Signals from Binary Neutron Star Coalescences with the Cherenkov Telescope Array: Prospects and Observing Strategies

S. Abe[1], J. Abhir[2], A. Abhishek[3], F. Acero[4,5], A. Acharyya[6], R. Adam[7,8], A. Aguasca-Cabot[9], I. Agudo[10], I. Albanese[11], J. Alfaro[12], C. Alispach[13], R. Alves Batista[14], E. Amato[15], G. Ambrosi[16], D. Ambrosino[17,18], F. Ambrosino[19], L. Angel[20,21], C. Aramo[17], A. Arbet-Engels[22], C. Arcaro[23], C. Arena[24], T. T. H. Arnesen[25], K. Asano[1], H. Ashkar[8,26], C. Bakshi[27], C. Balazs[28], M. Balbo[13], A. Baquero Larriva[29,30], V. Barbosa Martins[31], J. A. Barrio[29], C. Bartolini[32,33], I. Batković[11], R. Batzofin[34], N. Bavdaz[35], J. Becerra González[25,36], G. Beck[37], W. Benbow[38], E. Bernardini[11], M. G. Bernardini[39,40], J. Bernete[41], A. Berti[22], B. Bertucci[16], V. Beshley[42], P. Bhattacharjee[35], S. Bhattacharyya[35], C. Bigongiari[19,43], A. Biland[2], E. Bissaldi[44,45], M. Blaña[12], O. Blanch[46], J. Blazek[47], C. Boisson[48], G. Bonnoli[39,49], Z. Bosnjak[50], E. Bottacini[11], M. Böttcher[51], E. Bronzini[52], G. Brunelli[52], J. Buces Sáez[29], A. Bulgarelli[52], T. Bulik[53], L. Burmistrov[13], P. G. Calisse[54], A. Campoy-Ordaz[55], B. K. Cantlay[56,57], G. Capasso[58], A. Caproni[59], R. Capuzzo-Dolcetta[19,60], M. Cardillo[61], S. Caroff[62], A. Carosi[19], E. Carquin[63], S. Casanova[64], E. Cascone[58], F. Cassol[65], G. Castignani[52], F. Catalani[66], D. Cerasole[33], M. Cerruti[67], A. Cerviño Cortínez[29], P. M. Chadwick[68], S. Chaty[67], A. W. Chen[37], Y. Chen[69], M. Chernyakova[70], A. Chiavassa[71,72], G. Chon[22], J. Chudoba[47], L. Chytka[47], G. M. Cicciari[73,74], A. Cifuentes Santos[41], C. H. Coimbra Araujo[75], J. L. Contreras[29], B. Cornejo[76], J. Cortina[41], A. Costa[24], G. Cotter[77], P. Cristofari[48], O. Cuevas[78], Z. Curtis-Ginsberg[79], A. D'Aì[80], G. D'Amico[46], F. D'Ammando[81], P. D'Avanzo[39], P. Da Vela[52], L. David[82], F. Dazzi[83], M. de Bony de Lavergne[65], V. De Caprio[58], E. M. de Gouveia Dal Pino[84], B. De Lotto[85], M. de Naurois[8], V. de Souza[86], L. del Peral[87], M. V. del Valle[84], C. Delgado[41], D. della Volpe[13], D. Depaoli[54], A. Dettlaff[22], L. Di Bella[88], T. Di Girolamo[17,18], A. Di Piano[52], F. Di Pierro[71], R. Di Tria[45], L. Di Venere[45], R. Dima[11], A. Dinesh[29], E. Do Souto Espiñeira[41], D. Dominis Prester[89], A. Donini[19], D. Dorner[90], J. Dörner[91], M. Doro[11], L. Ducci[92], V. V. Dwarkadas[93], J. Ebr[47], C. Eckner[35], K. Egberts[34], L. Eisenberger[90], D. Elsässer[88], G. Emery[10], C. Escañuela Nieves[64], P. Escarate[94], M. Escobar Godoy[95], J. Escudero Pedrosa[38], P. Esposito[96,97], D. Falceta-Goncalves[98], E. Fedorova[19,99], S. Fegan[8], K. Feijen[67], Q. Feng[100], G. Ferrand[101,102], E. Fiandrini[16], A. Fiasson[62], M. Filipovic[103], V. Fioretti[52], L. Foffano[61], G. Fontaine[8], F. Frías García-Lago[25], Y. Fukazawa[104], Y. Fukui[105], G. Galanti[97], G. Galaz[12], S. Gallozzi[19], V. Gammaldi[106], S. García Soto[41], M. Garczarczyk[82], C. Gasbarra[19,43], D. Gasparrini[43], M. Gaug[55], G. Ghirlanda[39], J. G. Giesbrecht Formiga Paiva[107], N. Giglietto[44,45], F. Giordano[33], M. Giroletti[81], R. Giuffrida[4,108], J.-F. Glicenstein[76], P. Goldoni[67], J. M. González[109], J. Goulart Coelho[110], T. Gradetzke[88], J. Granot[111,112], R. Grau[1], D. Green[54], J. G. Green[22], J. Grube[113], J. Hackfeld[88,91], D. Hadasch[26], A. Hahn[22], P. Hamal[47], W. Hanlon[38], S. Hara[114], V. M. Harvey[115], T. Hassan[41], K. Hayashi[1,116], B. Hess[92], L. Heckmann[22,67], N. Hiroshima[1,117], B. Hnatyk[99], R. Hnatyk[99], D. Horan[8], P. Horvath[118], D. Hrupec[119], S. Hussain[35], M. Iarlori[120], T. Inada[1,121], F. Incardona[24], S. Inoue[1,122], F. Iocco[17,18], A. Iuliano[17], Jahanvi[85], M. Jamrozy[123], P. Janecek[47], F. Jankowsky[124], C. Jarnot[125], I. Jaroschewski[76], P. Jean[125], V. Jilek[47,118], I. Jiménez Martínez[22], J. Jimenez Quiles[46], W. Jin[69], E. Joshi[82], J. Jurysek[47], V. Karas[126], H. Katagiri[127], J. Kataoka[128], S. Kaufmann[68], T. Keita[4], D. Kerszberg[14], M. Kherlakian[31], D. B. Kieda[100], R. Kissmann[129], T. Kleiner[82], Y. Kobayashi[1,122], K. Kohri[130,131], D. Kolar[35], N. Komin[37], A. Kong[1], K. Kosack[4], D. Kostunin[82], G. Kowal[98], H. Kubo[1], J. Kushida[132], A. La Barbera[80], N. La Palombara[97], B. Lacave[13], M. Láinez[29], A. Lamastra[19], J. Lapington[133], S. Lazarević[103], J.-P. Lenain[14], F. Leone[134], E. Leonora[74], G. Leto[24], E. Lindfors[135], S. Lombardi[19], F. Longo[136], R. López-Coto[10], M. López-Moya[29], A. López-Oramas[25], J. Lozano Bahilo[87], P. L. Luque-Escamilla[137], E. Lyard[138], O. Macias[139], P. Majumdar[27], M. Makariev[140], D. Mandat[47], S. Mangano[41], A. Marchetti[39], M. Mariotti[11], S. Markoff[139,141], I. Márquez[10], G. Marsella[73,74], J. Martí[137], D. Martín Domínguez[29], M. Martínez[46], O. Martinez[142,143], G. Maurin[62], D. Mazin[1,22], D. Melkumyan[82], S. Menon[19,144], E. Mestre[26], D. M.-A. Meyer[26], D. Miceli[23], M. Miceli[73,108], M. Michailidis[145,146], T. Miener[13], J. M. Miranda[143,147], R. Moderski[148], M. Molero[41], C. Molfese[83], E. Molina[25], K. Morik[88,149], A. Morselli[43], E. Moulin[76], A. L. Müller[47], K. Munari[24], T. Murach[82], A. Muraczewski[148], H. Muraishi[150], T. Nakamori[151], L. Nava[39], R. Nemmen[84,145], J. Niemiec[152], D. Nieto[29], M. Nievas Rosillo[25], M. Nikołajuk[153], L. Nikolić[3], K. Noda[1,122], D. Nosek[154], V. Novotny[154], S. Nozaki[1], A. Okumura[155,156], R. A. Ong[69], R. Orito[157], M. Orlandini[52], E. Orlando[136], S. Orlando[108], J. Otero-Santos[23], I. Oya[41], M. Ozlati Moghadam[34], A. Pagliaro[80], M. Palatiello[19], A. Pandey[100], G. Panebianco[52], D. Paneque[22], F. R. Pantaleo[44,45], J. M. Paredes[9], B. Patricelli[19,158], A. Pe'er[22], M. Pech[47], M. Pecimotika[46], M. Peresano[22], E. Peretti[15,67], J. Pérez-Romero[35], G. Peron[15], F. Perrotta[58], M. Persic[159,160], O. Petruk[42,108], F. Pfeifle[90], E. Pietropaolo[161], M. Pihet[10], L. Pinchbeck[28], F. Pintore[80], G. Pirola[22], C. Pittori[19,43], F. Podobnik[13], M. Pohl[34], V. Pollet[62], G. Ponti[39], E. Prandini[11], G. Principe[136], M. Prouza[47], E. Pueschel[31], G. Pühlhofer[92], M. L. Pumo[74,134], M. Punch[67], A. Quirrenbach[124], S. Rainò[33], R. Rando[11], S. Recchia[15,152], A. Reimer[129], O. Reimer[129],

I. Reis[76,86], A. Reisenegger[12,162], W. Rhode[88], M. Ribó[9], C. Ricci[138,163], T. Richtler[164], J. Rico[46], L. Riitano[79], V. Rizi[161], E. Roache[38], G. Rodriguez Fernandez[43], J. J. Rodríguez-Vázquez[41], P. Romano[39], G. Romeo[24], J. Rosado[29], A. Rosales de Leon[165], A. Roy[166], I. Sadeh[82], L. Saha[38], T. Saito[1], M. Sánchez-Conde[167], P. Sangiorgi[80], H. Sano[1,168], R. Santos-Lima[84], V. Sapienza[73,108], S. Sarkar[77], F. G. Saturni[19], A. Scherer[169], F. Schiavone[33], P. Schipani[58], P. Schovanek[47], F. Schussler[76], M. Seglar Arroyo[46], O. Sergijenko[99,170,171], H. Siejkowski[172], A. Simongini[83,144], V. Sliusar[138], A. Slowikowska[173], I. Sofia[64,71], H. Sol[48], S. Spinello[24], A. Stamerra[19,43], S. Stanič[35], T. Starecki[174], R. Starling[133], Ł. Stawarz[123], T. Stolarczyk[4], Y. Suda[104], A. Sunny[61,144], T. Suomijarvi[175], R. Takeishi[1], S. J. Tanaka[176], F. Tavecchio[39], T. Tavernier[47], Y. Terada[177,178], M. Teshima[22], V. Testa[19], W. W. Tian[1,179], Y. Tian[82], L. Tibaldo[125], O. Tibolla[68], S. J. Tingay[180], C. J. Todero Peixoto[66,86], F. Tombesi[43,144], D. Tonev[140], F. Torradeflot[41,181], D. F. Torres[26], N. Tothill[103], G. Tovmassian[182], G. Tripodo[73], A. Trois[183], A. Tsiahina[125], A. Tutone[80], L. Vaclavek[47,118], M. Vacula[47,118], C. van Eldik[184], J. Vandenbroucke[79], V. Vassiliev[69], M. Vázquez Acosta[25], M. Vecchi[185], S. Vercellone[39], S. D. Vergani[48], I. Viale[71], A. Viana[86], A. Vigliano[85], J. Vignatti[186], C. F. Vigorito[71,72], J. Villanueva[78], E. Visentin[71,72], V. Voitsekhovskyi[139], S. Vorobiov[35], I. Vovk[1], T. Vuillaume[62], R. Walter[138], M. Wechakama[56,57], M. White[115], A. Wierzcholska[152], M. Will[54], F. Wohlleben[64], A. Wolter[39], F. Xotta[35], T. Yamamoto[187], R. Yamazaki[176], T. Yoshikoshi[1], M. Zacharias[124], G. Zaharijas[35], R. Zanmar Sanchez[24,58], D. Zavrtanik[35], M. Zavrtanik[35], A. Zech[48], V. I. Zhdanov[99], M. Živec[35], and J. Zuriaga-Puig[167]

(CTAO Consortium)

and

A. Colombo[19,60]

[1] Institute for Cosmic Ray Research, University of Tokyo, 5-1-5, Kashiwa-no-ha, Kashiwa, Chiba 277-8582, Japan
[2] ETH Zürich, Institute for Particle Physics and Astrophysics, Otto-Stern-Weg 5, 8093 Zürich, Switzerland
[3] INFN and Università degli Studi di Siena, Dipartimento di Scienze Fisiche, della Terra e dell'Ambiente (DSFTA), Sezione di Fisica, Via Roma 56, 53100 Siena, Italy
[4] Université Paris-Saclay, Université Paris Cité, CEA, CNRS, AIM, F-91191 Gif-sur-Yvette Cedex, France
[5] FSLAC IRL 2009, CNRS/IAC, La Laguna, Tenerife, Spain
[6] University of Alabama, Tuscaloosa, Department of Physics and Astronomy, Gallalee Hall, Box 870324 Tuscaloosa, AL 35487-0324, USA
[7] Université Côte d'Azur, Observatoire de la Côte d'Azur, CNRS, Laboratoire Lagrange, France
[8] Laboratoire Leprince-Ringuet, CNRS/IN2P3, École polytechnique, Institut Polytechnique de Paris, 91120 Palaiseau, France
[9] Departament de Física Quàntica i Astrofísica, Institut de Ciències del Cosmos, Universitat de Barcelona, IEEC-UB, Martí i Franquès, 1, 08028, Barcelona, Spain
[10] Instituto de Astrofísica de Andalucía-CSIC, Glorieta de la Astronomía s/n, 18008, Granada, Spain
[11] INFN Sezione di Padova and Università degli Studi di Padova, Via Marzolo 8, 35131 Padova, Italy
[12] Pontificia Universidad Católica de Chile, Av. Libertador Bernardo O'Higgins 340, Santiago, Chile
[13] Département de physique nucléaire et corpusculaire, University de Genève, Faculté de Sciences, 1205 Genève, Switzerland
[14] Sorbonne Université, CNRS/IN2P3, Laboratoire de Physique Nucléaire et de Hautes Energies, LPNHE, 4 place Jussieu, 75005 Paris, France
[15] INAF - Osservatorio Astrofisico di Arcetri, Largo E. Fermi, 5 - 50125 Firenze, Italy
[16] INFN Sezione di Perugia and Università degli Studi di Perugia, Via A. Pascoli, 06123 Perugia, Italy
[17] INFN Sezione di Napoli, Via Cintia, ed. G, 80126 Napoli, Italy
[18] Università degli Studi di Napoli "Federico II"—Dipartimento di Fisica "E. Pancini", Complesso Universitario di Monte Sant'Angelo, Via Cintia - 80126 Napoli, Italy
[19] INAF - Osservatorio Astronomico di Roma, Via di Frascati 33, 00078, Monteporzio Catone, Italy; barbara.patricelli@inaf.it, antonio.stamerra@inaf.it
[20] International Institute of Physics, Universidade Federal do Rio Grande do Norte, 59078-970, Natal, RN, Brasil
[21] Departamento de Física, Universidade Federal do Rio Grande do Norte, 59078-970, Natal, RN, Brasil
[22] Max-Planck-Institut für Physik, Boltzmannstraße 8, 85748 Garching, Germany; jgreen@mpp.mpg.de
[23] INFN Sezione di Padova, Via Marzolo 8, 35131 Padova, Italy
[24] INAF—Osservatorio Astrofisico di Catania, Via Santa Sofia, 78, 95123 Catania, Italy
[25] Instituto de Astrofísica de Canarias and Departamento de Astrofísica, Universidad de La Laguna, La Laguna, Tenerife, Spain
[26] Institute of Space Sciences (ICE, CSIC), and Institut d'Estudis Espacials de Catalunya (IEEC), and Institució Catalana de Recerca I Estudis Avançats (ICREA), Campus UAB, Carrer de Can Magrans, s/n 08193 Cerdanyola del Vallés, Spain
[27] Saha Institute of Nuclear Physics, A CI of Homi Bhabha National Institute, Kolkata 700064, West Bengal, India
[28] School of Physics and Astronomy, Monash University, Melbourne, Victoria 3800, Australia
[29] IPARCOS-UCM, Instituto de Física de Partículas y del Cosmos, and EMFTEL Department, Universidad Complutense de Madrid, E-28040 Madrid, Spain
[30] Faculty of Science and Technology, Universidad del Azuay, Cuenca, Ecuador
[31] Ruhr University Bochum, Faculty of Physics and Astronomy, Astronomical Institute (AIRUB), Universitätsstraße 150, 44801 Bochum, Germany
[32] Università degli Studi di Trento, Via Calepina, 14, 38122 Trento, Italy
[33] INFN Sezione di Bari and Università degli Studi di Bari, via Orabona 4, 70124 Bari, Italy
[34] Institut für Physik & Astronomie, Universität Potsdam, Karl-Liebknecht-Strasse 24/25, 14476 Potsdam, Germany
[35] Center for Astrophysics and Cosmology (CAC), University of Nova Gorica, Nova Gorica, Slovenia
[36] Consejo Superior de Investigaciones Científicas (CSIC), 28006 Madrid, Spain
[37] University of the Witwatersrand, 1 Jan Smuts Avenue, Braamfontein, 2000 Johannesburg, South Africa
[38] Center for Astrophysics | Harvard & Smithsonian, 60 Garden Street, Cambridge, MA 02138, USA
[39] INAF—Osservatorio Astronomico di Brera, Via Brera 28, 20121 Milano, Italy; lara.nava@ts.infn.it
[40] Laboratoire Univers et Particules de Montpellier, Université de Montpellier, CNRS/IN2P3, CC 72, Place Eugène Bataillon, F-34095 Montpellier Cedex 5, France
[41] CIEMAT, Avenida Complutense 40, 28040 Madrid, Spain
[42] Pidstryhach Institute for Applied Problems in Mechanics and Mathematics NASU, 3B Naukova Street, Lviv, 79060, Ukraine
[43] INFN Sezione di Roma Tor Vergata, Via della Ricerca Scientifica 1, 00133 Rome, Italy
[44] Politecnico di Bari, via Orabona 4, 70124 Bari, Italy
[45] INFN Sezione di Bari, via Orabona 4, 70126 Bari, Italy
[46] Institut de Fisica d'Altes Energies (IFAE), The Barcelona Institute of Science and Technology, Campus UAB, 08193, Bellaterra (Barcelona), Spain; mseglar@ifae.es

[47] FZU - Institute of Physics of the Czech Academy of Sciences, Na Slovance 1999/2, 182 00 Praha 8, Czech Republic
[48] LUX, Observatoire de Paris, Université PSL, Sorbonne Université, CNRS, 5 place Jules Janssen, 92190, Meudon, France
[49] INFN Sezione di Pisa, Edificio C–Polo Fibonacci, Largo Bruno Pontecorvo 3, 56127, Pisa, Italy
[50] University of Zagreb, Faculty of Electrical Engineering and Computing, Unska 3, 10000 Zagreb, Croatia
[51] Centre for Space Research, North-West University, Potchefstroom, 2520, South Africa
[52] INAF - Osservatorio di Astrofisica e Scienza dello spazio di Bologna, Via Piero Gobetti 93/3, 40129 Bologna, Italy
[53] Astronomical Observatory, Department of Physics, University of Warsaw, Aleje Ujazdowskie 4, 00478 Warsaw, Poland
[54] CTAO, Via Piero Gobetti 93/3, 40129 Bologna, Italy
[55] Unitat de Física de les Radiacions, Departament de Física, and CERES-IEEC, Universitat Autònoma de Barcelona, Edifici C3, Campus UAB, 08193 Bellaterra, Spain
[56] Department of Physics, Faculty of Science, Kasetsart University, 50 Ngam Wong Wan Road, Lat Yao, Chatuchak, Bangkok, 10900, Thailand
[57] National Astronomical Research Institute of Thailand, 191 Huay Kaew Rdoa, Suthep, Muang, Chiang Mai, 50200, Thailand
[58] INAF—Osservatorio Astronomico di Capodimonte, Via Salita Moiariello 16, 80131 Napoli, Italy
[59] Universidade Cidade de São Paulo, Núcleo de Astrofísica, R. Galvão Bueno 868, Liberdade, São Paulo, SP, 01506-000, Brazil
[60] Dep. of Physics, Sapienza, University of Roma, Piazzale A. Moro 5, 00185, Roma, Italy
[61] INAF—Istituto di Astrofisica e Planetologia Spaziali (IAPS), Via del Fosso del Cavaliere 100, 00133 Roma, Italy
[62] Univ. Savoie Mont Blanc, CNRS, Laboratoire d'Annecy de Physique des Particules - IN2P3, 74000 Annecy, France
[63] CCTVal, Universidad Técnica Federico Santa María, Avenida España 1680, Valparaíso, Chile
[64] Max-Planck-Institut für Kernphysik, Saupfercheckweg 1, 69117 Heidelberg, Germany
[65] Aix Marseille Univ, CNRS/IN2P3, CPPM, Marseille, France
[66] Escola de Engenharia de Lorena, Universidade de São Paulo, Área I - Estrada Municipal do Campinho, s/n°, CEP 12602-810, Ponte Nova, Lorena, Brazil
[67] Université Paris Cité, CNRS, Astroparticule et Cosmologie, F-75013 Paris, France
[68] Centre for Advanced Instrumentation, Department of Physics, Durham University, South Road, Durham, DH1 3LE, UK
[69] Department of Physics and Astronomy, University of California, Los Angeles, CA 90095, USA
[70] Dublin City University, Glasnevin, Dublin 9, Ireland
[71] INFN Sezione di Torino, Via P. Giuria 1, 10125 Torino, Italy
[72] Dipartimento di Fisica - Università degli Studi di Torino, Via Pietro Giuria 1 - 10125 Torino, Italy
[73] Dipartimento di Fisica e Chimica "E. Segrè," Università degli Studi di Palermo, Via Archirafi 36, 90123, Palermo, Italy
[74] INFN Sezione di Catania, Via Santa Sofia 64, 95123 Catania, Italy
[75] Universidade Federal Do Paraná - Setor Palotina, Departamento de Engenharias e Exatas, Rua Pioneiro, 2153, Jardim Dallas, CEP: 85950-000 Palotina, Paraná, Brazil
[76] IRFU, CEA, Université Paris-Saclay, Bât 141, 91191, Gif-sur-Yvette, France; fabian.schussler@cea.fr
[77] University of Oxford, Department of Physics, Clarendon Laboratory, Parks Road, Oxford, OX1 3PU, UK
[78] Universidad de Valparaíso, Blanco 951, Valparaiso, Chile
[79] University of Wisconsin, Madison, 500 Lincoln Drive, Madison, WI, 53706, USA
[80] INAF—Istituto di Astrofisica Spaziale e Fisica Cosmica di Palermo, Via Ugo La Malfa 153, 90146 Palermo, Italy
[81] INAF—Istituto di Radioastronomia, Via Gobetti 101, 40129 Bologna, Italy
[82] Deutsches Elektronen-Synchrotron, Platanenallee 6, 15738 Zeuthen, Germany
[83] INAF—Istituto Nazionale di Astrofisica, Viale del Parco Mellini 84, 00136 Rome, Italy
[84] Instituto de Astronomia, Geofísica e Ciências Atmosféricas - Universidade de São Paulo, Cidade Universitária, Rua do Matão, 1226, CEP 05508-090, São Paulo, SP, Brazil
[85] INFN Sezione di Trieste and Università degli Studi di Udine, Via delle Scienze 208, 33100 Udine, Italy
[86] Instituto de Física de São Carlos, Universidade de São Paulo, Avenida Trabalhador São-carlense, 400 - CEP 13566-590, São Carlos, SP, Brazil
[87] Universidad de Alcalá - Space & Astroparticle group, Facultad de Ciencias, Campus Universitario Carretera Madrid-Barcelona, Km. 33.600 28871 Alcalá de Henares (Madrid), Spain
[88] Astroparticle Physics, Department of Physics, TU Dortmund University, Otto-Hahn-Straße 4a, 44227 Dortmund, Germany
[89] University of Rijeka, Faculty of Physics, Radmile Matejcic 2, 51000 Rijeka, Croatia
[90] Institute for Theoretical Physics and Astrophysics, Universität Würzburg, Campus Hubland Nord, Emil-Fischer-Straße 31, 97074, Würzburg, Germany
[91] Institut für Theoretische Physik, Lehrstuhl IV: Plasma-Astroteilchenphysik, Ruhr-Universität Bochum, Universitätsstraße 150, 44801 Bochum, Germany
[92] Institut für Astronomie und Astrophysik, Universität Tübingen, Sand 1, 72076, Tübingen, Germany
[93] Department of Astronomy and Astrophysics, University of Chicago, 5640 S Ellis Avenue, Chicago, IL, 60637, USA
[94] Escuela de Ingeniería Eléctrica, Facultad de Ingeniería, Pontificia Universidad Católica de Valparaíso, Avenida Brasil 2147, Valparaíso, Chile
[95] Santa Cruz Institute for Particle Physics and Department of Physics, University of California, Santa Cruz, 1156 High Street, Santa Cruz, CA 95064, USA
[96] University School for Advanced Studies IUSS Pavia, Palazzo del Broletto, Piazza della Vittoria 15, 27100 Pavia, Italy
[97] INAF—Istituto di Astrofisica Spaziale e Fisica Cosmica di Milano, Via Adolfo Corti 12, 20133 Milano, Italy
[98] Escola de Artes, Ciências e Humanidades, Universidade de São Paulo, Rua Arlindo Bettio, CEP 03828-000, 1000 São Paulo, Brazil
[99] Astronomical Observatory of Taras Shevchenko National University of Kyiv, 3 Observatorna Street, Kyiv, 04053, Ukraine
[100] Department of Physics and Astronomy, University of Utah, Salt Lake City, UT 84112-0830, USA
[101] The University of Manitoba, Dept of Physics and Astronomy, Winnipeg, Manitoba R3T 2N2, Canada
[102] RIKEN, Institute of Physical and Chemical Research, 2-1 Hirosawa, Wako, Saitama, 351-0198, Japan
[103] Western Sydney University, Locked Bag 1797, Penrith, NSW 2751, Australia
[104] Physics Program, Graduate School of Advanced Science and Engineering, Hiroshima University, 739-8526 Hiroshima, Japan
[105] Department of Physics, Nagoya University, Chikusa-ku, Nagoya, 464-8602, Japan
[106] Department of Information Technology, Escuela Politécnica Superior, Universidad San Pablo-CEU, CEU Universities, Campus Montepríncipe, Boadilla del Monte, Madrid 28668, Spain
[107] Centro Brasileiro de Pesquisas Físicas, Rua Xavier Sigaud 150, RJ 22290-180, Rio de Janeiro, Brazil
[108] INAF—Osservatorio Astronomico di Palermo "G.S. Vaiana", Piazza del Parlamento 1, 90134 Palermo, Italy
[109] Universidad Andrés Bello, Avenida Fernández Concha 700, Las Condes, Santiago, Chile
[110] Núcleo de Astrofísica e Cosmologia (Cosmo-ufes) & Departamento de Física, Universidade Federal do Espírito Santo (UFES), Avenida Fernando Ferrari, 514. 29065-910. Vitória-ES, Brazil
[111] Astrophysics Research Center of the Open University (ARCO), The Open University of Israel, P.O. Box 808, Ra'anana 4353701, Israel
[112] Department of Physics, The George Washington University, WA, DC 20052, USA
[113] King's College London, Strand, London, WC2R 2LS, UK
[114] General Education Center, Yamanashi-Gakuin University, Kofu, Yamanashi 400-8575, Japan
[115] School of Physics, Chemistry and Earth Sciences, University of Adelaide, Adelaide SA 5005, Australia
[116] Sendai College, National Institute of Technology, 4-16-1 Ayashi-Chuo, Aoba-ku, Sendai city, Miyagi 989-3128, Japan

[117] Department of Physics, Faculty of Engineering Science, Yokohama National University, Yokohama 240–8501, Japan
[118] Palacký University Olomouc, Faculty of Science, Joint Laboratory of Optics of Palacký University and Institute of Physics of the Czech Academy of Sciences, 17. listopadu 1192/12, 779 00 Olomouc, Czech Republic
[119] Josip Juraj Strossmayer University of Osijek, Trg Ljudevita Gaja 6, 31000 Osijek, Croatia
[120] CETEMPS Dipartimento di Scienze Fisiche e Chimiche, Università degli Studi dell'Aquila and GSGC-LNGS-INFN, Via Vetoio 1, L'Aquila, 67100, Italy
[121] Research Center for Advanced Particle Physics, Kyushu University, 744 Motooka, Nishi-ku, Fukuoka 819-0395, Japan
[122] Chiba University, 1-33, Yayoicho, Inage-ku, Chiba-shi, Chiba, 263-8522, Japan
[123] Astronomical Observatory, Jagiellonian University, ulica Orla 171, 30-244 Cracow, Poland
[124] Landessternwarte, Zentrum für Astronomie der Universität Heidelberg, Königstuhl 12, 69117 Heidelberg, Germany
[125] IRAP, Université de Toulouse, CNRS, CNES, UPS, 9 avenue Colonel Roche, 31028, Toulouse, Cedex 4, France
[126] Astronomical Institute of the Czech Academy of Sciences, Bocni II 1401 - 14100 Prague, Czech Republic
[127] Faculty of Science, Ibaraki University, Mito, Ibaraki, 310-8512, Japan
[128] Faculty of Science and Engineering, Waseda University, Shinjuku, Tokyo 169-8555, Japan
[129] Universität Innsbruck, Institut für Astro- und Teilchenphysik, Technikerstraße 25/8, 6020 Innsbruck, Austria
[130] National Astronomical Observatory of Japan (NAOJ), Division of Science, 2-21-1, Osawa, Mitaka, Tokyo 181-8588, Japan
[131] Institute of Particle and Nuclear Studies, KEK (High Energy Accelerator Research Organization), 1-1 Oho, Tsukuba, 305-0801, Japan
[132] Department of Physics, Tokai University, 4-1-1, Kita-Kaname, Hiratsuka, Kanagawa 259-1292, Japan
[133] School of Physics and Astronomy, University of Leicester, Leicester, LE1 7RH, UK
[134] Università degli studi di Catania, Dipartimento di Fisica e Astronomia "Ettore Majorana", Via S. Sofia 64, 95123 Catania, Italy
[135] Department of Physics and Astronomy, University of Turku, Finland, FI-20014 University of Turku, Finland
[136] INFN Sezione di Trieste and Università degli Studi di Trieste, Via Valerio 2 I, 34127 Trieste, Italy
[137] Escuela Politécnica Superior de Jaén, Universidad de Jaén, Campus Las Lagunillas s/n, Edif. A3, 23071, Jaén, Spain
[138] Department of Astronomy, University of Geneva, Chemin d'Ecogia 16, CH-1290 Versoix, Switzerland
[139] Anton Pannekoek Institute/GRAPPA, University of Amsterdam, Science Park 904 1098 XH Amsterdam, The Netherlands
[140] Institute for Nuclear Research and Nuclear Energy, Bulgarian Academy of Sciences, 72 boulevard Tsarigradsko chaussee, 1784 Sofia, Bulgaria
[141] University of Cambridge, Cambridge, UK
[142] Department of Biology and Geology, Physics and Inorganic Chemistry, Address: C/ Tulipán, s/n. 28933 Móstoles (Faculty of Experimental Sciences and Technology), Spain
[143] UCM-ELEC group, EMFTEL Department, University Complutense of Madrid, 28040 Madrid, Spain
[144] Macroarea di Scienze MMFFNN, Università di Roma Tor Vergata, Via della Ricerca Scientifica 1, 00133 Rome, Italy
[145] Kavli Institute for Particle Astrophysics and Cosmology, Stanford University, Stanford, CA 94305, USA
[146] Kavli Institute for Particle Astrophysics and Cosmology, Department of Physics and SLAC National Accelerator Laboratory, Stanford University, 2575 Sand Hill Road, Menlo Park, CA 94025, USA
[147] IPARCOS Institute, Faculty of Physics (UCM), 28040 Madrid, Spain
[148] Nicolaus Copernicus Astronomical Center, Polish Academy of Sciences, ulica Bartycka 18, 00-716 Warsaw, Poland
[149] Joseph-von-Fraunhofer-Str. 25, 44227 Dortmund, Germany
[150] School of Allied Health Sciences, Kitasato University, Sagamihara, Kanagawa 228-8555, Japan
[151] Department of Physics, Yamagata University, Yamagata, Yamagata 990-8560, Japan
[152] The Henryk Niewodniczański Institute of Nuclear Physics, Polish Academy of Sciences, ulica Radzikowskiego 152, 31-342 Cracow, Poland
[153] University of Białystok, Faculty of Physics, ul. K. Ciołkowskiego 1L, 15-245 Białystok, Poland
[154] Charles University, Institute of Particle & Nuclear Physics, V Holešovičkách 2, 180 00 Prague 8, Czech Republic
[155] Institute for Space—Earth Environmental Research, Nagoya University, Furo-cho, Chikusa-ku, Nagoya 464-8601, Japan
[156] Kobayashi—Maskawa Institute for the Origin of Particles and the Universe, Nagoya University, Furo-cho, Chikusa-ku, Nagoya 464-8602, Japan
[157] Graduate School of Technology, Industrial and Social Sciences, Tokushima University, Tokushima 770-8506, Japan
[158] University of Pisa, Largo Bruno Pontecorvo 3, 56127 Pisa, Italy
[159] INAF—Osservatorio Astronomico di Padova, Vicolo dell'Osservatorio 5, 35122 Padova, Italy
[160] INAF—Osservatorio Astronomico di Padova and INFN Sezione di Trieste, gruppo collegamento Udine, Via delle Scienze 208 I-33100 Udine, Italy
[161] Dipartimento di Scienze Fisiche e Chimiche, Università degli Studi dell'Aquila and GSGC-LNGS-INFN, Via Vetoio 1, L'Aquila, 67100, Italy
[162] Departamento de Física, Facultad de Ciencias Básicas, Universidad Metropolitana de Ciencias de la Educación, Avenida José Pedro Alessandri 774, Ñuñoa, Santiago, Chile
[163] Instituto de Estudios Astrofísicos, Facultad de Ingeniería y Ciencias, Universidad Diego Portales, Avenida Ejército Libertador 441, 8370191 Santiago, Chile
[164] Departamento de Astronomía, Universidad de Concepción, Barrio Universitario S/N, Concepción, Chile
[165] Faculty of Physics and Applied Computer Science, University of Lódź, ulica Pomorska 149-153, 90-236 Lódź, Poland
[166] Hiroshima Astrophysical Science Center, Hiroshima University, Higashi-Hiroshima, Hiroshima 739-8526, Japan
[167] Instituto de Física Teórica UAM/CSIC and Departamento de Física Teórica, Universidad Autónoma de Madrid, c/ Nicolás Cabrera 13-15, Campus de Cantoblanco UAM, 28049 Madrid, Spain
[168] Gifu University, Faculty of Engineering, 1-1 Yanagido, Gifu 501-1193, Japan
[169] Departamento de Física, Universidad de Santiago de Chile (USACH), Avenida Victor Jara 3493, Estación Central, Santiago, Chile
[170] Main Astronomical Observatory of the National Academy of Sciences of Ukraine, Zabolotnoho Street, 27, 03143, Kyiv, Ukraine
[171] Faculty of Space Technologies, AGH University of Krakow, Aleja Mickiewicza 30, Kraków 30-059, Poland
[172] Academic Computer Centre CYFRONET AGH, ulica Nawojki 11, 30-950, Kraków, Poland
[173] Institute of Astronomy, Faculty of Physics, Astronomy and Informatics, Nicolaus Copernicus University in Toruń, ulica Grudzidzka 5, 87-100 Toruń, Poland
[174] Warsaw University of Technology, Faculty of Electronics and Information Technology, Institute of Electronic Systems, Nowowiejska 15/19, 00-665 Warsaw, Poland
[175] Université Paris-Saclay, CNRS/IN2P3, IJCLab, 91405 Orsay, France
[176] Department of Physical Sciences, Aoyama Gakuin University, Fuchinobe, Sagamihara, Kanagawa, 252-5258, Japan
[177] Graduate School of Science and Engineering, Saitama University, 255 Simo-Ohkubo, Sakura-ku, Saitama city, Saitama 338-8570, Japan
[178] Institute of Space and Astronautical Science, JAXA, 3-1-4, Yoshinodai, Sagamihara, Kanagawa 229-8510, Japan
[179] School of Physics and Astronomy, Sun Yat-sen University, Zhuhai, People's Republic of China
[180] Curtin University, Kent Street, Bentley WA 6102, Australia
[181] Port d'Informació Científica, Edifici D, Carrer de l'Albareda, 08193, Bellaterrra (Cerdanyola del Vallès), Spain
[182] Universidad Nacional Autónoma de México, Delegación Coyoacán, 04510, Ciudad de México, Mexico
[183] INAF - Osservatorio Astronomico di Cagliari, Via della Scienza 5, I-09047 Selargius (CA), Italy
[184] Friedrich-Alexander-Universität Erlangen-Nürnberg, Erlangen Centre for Astroparticle Physics, Nikolaus-Fiebiger-Straße 2, 91058 Erlangen, Germany

[185] Kapteyn Astronomical Institute, University of Groningen, Landleven 12, 9747 AD, Groningen, The Netherlands
[186] Departamento de Física, Universidad Técnica Federico Santa María, Avenida España, 1680 Valparaíso, Chile
[187] Department of Physics, Konan University, Kobe, Hyogo, 658-8501, Japan
*Received 2026 February 21; revised 2026 April 9; accepted 2026 April 13; published 2026 June 3*

## Abstract

The detection of gravitational waves (GWs) from a binary neutron star (BNS) merger by Advanced LIGO and Advanced Virgo (GW170817), together with its electromagnetic counterpart, the short gamma-ray burst GRB 170817A, heralded the birth of multimessenger astronomy. The detection of TeV emission from GRBs motivates follow-up observations with the Cherenkov Telescope Array Observatory (CTAO), which is ideal for detecting such signals due to its unprecedented sensitivity, rapid response, and wide-field survey capabilities. The aim of this work is to evaluate GeV–TeV GW follow-up strategies for CTAO using a multistep simulation pipeline and to estimate the expected rate of joint GW–GRB detections during observing run O5. Using a simulated sample of BNS systems with corresponding GW detections, gamma-ray emission is simulated through phenomenological prescriptions based on the observed population of short GRBs, including off-axis jet scenarios. CTAO observations are simulated to account for instrument response, sky tiling strategies, integration times, and varying observing conditions. Strategies with variable and constant integration times are investigated. We find that, via an optimized follow-up strategy, about 5% of simulated GW-associated short GRBs produce GeV–TeV radiation detectable by CTAO. Detectability is strongly influenced by the jet opening angle and viewing angle, suggesting that even rough estimates of the viewing angle in GW alerts could enhance targeting. This framework motivates future follow-ups of GW-detectable events, including neutron star–black hole mergers, and further supports the development of advanced strategies incorporating galaxy distributions and synergies with future detectors such as the Einstein Telescope.

*Unified Astronomy Thesaurus concepts:* Gamma-ray transient sources (1853); Gamma-ray telescopes (634); Gravitational wave astronomy (675); High energy astrophysics (739); Gamma-ray bursts (629); Gravitational wave sources (677)

## 1. Introduction

On 2017 August 17 a gravitational wave (GW) signal from the inspiral of a binary neutron star (BNS) merger was observed for the first time (B. P. Abbott et al. 2017a) by Advanced LIGO (LIGO Scientific Collaboration et al. 2015) and Advanced Virgo (F. Acernese et al. 2015); ∼2 s after this GW event, Fermi (A. Goldstein et al. 2017) and INTEGRAL (V. Savchenko et al. 2017) detected a short gamma-ray burst (GRB) in GRB 170817A. The association of GW170817 and GRB 170817A represents the first direct evidence that BNS mergers can produce short GRBs (sGRBs), confirmed by the very long baseline interferometry (VLBI) observations of a successful, structured jet (G. Ghirlanda et al. 2019). Long GRBs produce gamma-ray photons reaching TeV energies, as proven by the recent observations of GRB 190114C, GRB 201216C, and GRB 201015A by MAGIC (MAGIC Collaboration et al. 2019a; H. Abe et al. 2024; O. Blanch et al. 2020); GRB 180720B and GRB 190829A by H.E.S.S. (H. Abdalla et al. 2019; H. E. S. S. Collaboration et al. 2021); and GRB 221009A by LHAASO (Z. Cao et al. 2023; LHAASO Collaboration et al. 2023). Delayed by bright moonlight until 1.33 days postevent, observations of GRB 221009A using LST-1, the first large-sized telescope of the upcoming Cherenkov Telescope Array Observatory (CTAO), reached a significance of 4.1$\sigma$, resulting in the derivation of upper limits (K. Abe et al. 2025a). Finally, MAGIC observed the short GRB 160821B, obtaining a hint of TeV emission at a 3$\sigma$ level (V. A. Acciari et al. 2021). Motivated by these results, the scope of this work is to determine not only the prospects of joint GW–GRB detections with CTAO but also how the choice of observational strategy affects these prospects.

### 1.1. The Cherenkov Telescope Array Observatory

CTAO is poised to be the next generation of Imaging Atmospheric Cherenkov Telescopes (IACTs), covering a range in the very-high-energy (VHE) gamma-ray regime between 20 GeV and 300 TeV (see B. S. Acharya et al. 2013). So far, no VHE emission coincident with a GW event has been observed in the VHE band by any IACT. Upper limits were derived in the case of GW170817, both several hours (H. Abdalla et al. 2017) and months postmerger (H. Abdalla et al. 2020; O. S. Salafia et al. 2022b). Instead, in the case of GRB 211211A, a joint detection of kilonova emission was reported at a distance of ∼350 Mpc, closely resembling AT2017g, the kilonova counterpart to GW170817, together with GeV emission by Fermi-LAT (J. C. Rastinejad et al. 2022). During this period, the GW interferometer network was undergoing commissioning toward observing run O4, and consequently no GW detection was possible.

CTAO will provide an order of magnitude improvement in sensitivity compared to the current generation of IACTs, swift slewing capabilities reaching 180°/20 s, and a large field of view (FoV) between 4° and 10° depending on the telescope: these characteristics make it an ideal instrument to search for VHE emission from short GRBs associated to GW events.

### 1.2. LIGO–Virgo–KAGRA and IACTs

The fourth LIGO–Virgo–KAGRA (LVK) observing run started on 2023 May 24 and finished on 2025 November 18.[188] Upgrades of Advanced LIGO, Advanced Virgo, and KAGRA



[188] https://observing.docs.ligo.org/plan/

(T. Akutsu et al. 2019) interferometers will improve the broadband sensitivity toward the fifth LVK observing run, O5, which is currently planned for the beginning of 2028, a timeline consistent with the schedule of CTAO. The increased sensitivity will allow us to explore a much wider volume of the Universe, with the consequent increase in the GW detection rate (P. Petrov et al. 2022) and potentially in the multi-messenger detection rate with respect to the previous observing runs.

Yet, even with improved sensitivity in current and next-generation GW interferometers, significant localization uncertainties will persist for a large fraction of detections, largely depending on the size of the detector network. Improvements throughout the years on observation strategies (e.g., L. P. Singer et al. 2025) and observation campaign coordination tools (e.g., S. D. Wyatt et al. 2020) are key to maximizing the detection odds of the counterparts of GW detections, such as those from compact binary coalescences (CBCs). These automatic handling and scheduling strategies are crucial in small and medium-sized FoV telescopes, as in the case of the IACT, and have been optimized to cover rapidly large regions in the sky, as shown in H. Ashkar et al. (2021). In addition, recent GW follow-ups by IACTs have been shown to have the potential to cover a large portion of the uncertainty region of GW, as shown by the combined LST-1 and MAGIC observations of S241125n (D. Paneque et al. 2024), putting upper limits on the gamma-ray emission above 300 GeV, proving the capabilities of TeV observations to set useful constraints to the emission models. (MAGIC and LST-1 collaborations 2026 , in preparation).

### 1.3. GW Follow-up Campaigns

The capability of CTAO to perform the electromagnetic (EM) follow-up of GW events, as well as possible observational strategies, has already been studied in a few works (I. Bartos et al. 2018, B. Patricelli et al. 2018). In particular, B. Patricelli et al. (2018) investigated the prospects for joint GW and VHE EM observations with Advanced Virgo, Advanced LIGO, and CTAO, based on detailed simulations of BNS merger accompanied by short GRBs, with a focus on o n-axis sources. These refer to GRBs observed within the opening angle of the jet, as opposed to off-axis, which are those observed from outside the opening angle of the jet. They proposed an optimized observational strategy for CTAO EM follow-up of GW events, involving increasing exposure times for consecutive observations, and demonstrated that this approach enhances the likelihood of detecting VHE EM counterparts. Other works (I. Bartos et al. 2014, I. Bartos et al. 2019, B. Banerjee et al. 2023, T. Mondal et al. 2025) explored the capability of CTAO to follow-up GW events and to detect the electromagnetic counterparts in the VHE domain. In I. Bartos et al. (2014), the authors focused on poorly localized sources, demonstrating that CTAO will be able to detect short GRBs associated with GW events even if it needs to survey a sky area of $\sim$1000 deg$^2$ and if the observations are delayed by $\sim$100 s following the onset of gamma-ray emission. The prospects for CTAO with the next generation of GW interferometers such as the Einstein Telescope[189] have been briefly explored (B. Banerjee et al. 2023, A. Colombo et al. 2025). Interestingly, B. Banerjee et al. (2023) showed that early warning GW alerts—i.e., alerts issued prior to the merger of a binary system—could enable the detection of early VHE emission with CTAO. Conversely, other studies (C. Pellouin & F. Daigne 2024; J. P. Hope et al. 2025) have attempted to model the high-energy gamma-ray components of the GRB associated with GW170817, reaching differing conclusions regarding the detectability of VHE emission from the associated off-axis and on-axis GRBs. C. Yuan et al. (2022) examined the scenario of compact-object mergers embedded within the disk of an active galactic nucleus (AGN), where the predominant contribution to the gamma-ray emission would originate from external inverse Compton scattering of isotropic thermal photons from the disk. Their prospects show that for long-lasting jets of $T_{\rm dur} \sim 10^2$–$10^3$ s, CTAO will be able to detect 25–100 GeV emission out to a redshift $z = 1$. Recent work has explored the potential of detecting EM signals from stochastic GW backgrounds using a time-domain cross-correlation approach (H. J. Kuralkar et al. 2025), which is complementary to the approach described in this work, that focuses on matched-filtering-detected CBCs with two neutron stars as compact objects.

### 1.4. VHE Emission of Short GRBs

Short and long GRBs are expected to have different progenitors: long GRBs are associated with core-collapse of massive stars, while short GRBs are associated with the merger of compact binaries containing at least a neutron star (NS; E. Berger 2014; see, however, J. C. Rastinejad et al. 2022; A. J. Levan et al. 2024).

The existence of VHE emission—extending beyond 10 TeV—has been observed in long GRBs, i.e., from on-axis beamed jets produced after the collapse of the central object. Given the possibility of a similar jet structure in both long and short GRBs (G. Ghirlanda et al. 2011), TeV emission may be a common feature in short GRBs, yet this remains to be confirmed. The prevailing physical explanation for this emission is that VHE photons are produced via the synchrotron self-Compton (SSC) process at the shock formed in the afterglow phase by the interaction of the relativistic jet with the interstellar medium (ISM; see e.g., MAGIC Collaboration et al. 2019b and D. Miceli & L. Nava 2022 for a more extended list of references). The detectability of VHE photons from GW counterparts depends on several poorly constrained factors, including the microphysics driving jet processes, the geometry of the jetted emission (e.g., jet opening angle and structure), and the properties of the surrounding environment, such as the ISM density and distribution.

The EM counterparts of GW events are believed to be produced in both on-axis and off-axis GRBs, when structured jets are assumed (A. Kathirgamaraju et al. 2018), as confirmed by VLBI observations of GW170817 (G. Ghirlanda et al. 2019). The detailed structure of the jet affects off-axis observations by introducing a delay in the peak of the afterglow emission and causing an energy-dependent shift in the prompt emission (O. S. Salafia & G. Ghirlanda 2022; Ž. Bošnjak et al. 2024). These effects also depend on the jet opening angle, for which only limited constraints are currently available (W. Fong et al. 2015; A. Rouco Escorial et al. 2023).

The VHE emission is sensitive to these parameters, and constraining it provides unique postmerger signatures that are inaccessible in other EM bands. This work further investigates

[189] https://www.et-gw.eu/

their impact on the detectability of the jetted emission from GW events with CTAO.

### 1.5. This Work

Compared to previous work, we implemented a complete simulation chain, starting from GW events originating from BNS mergers and detectable by the LVK instruments during the O5 observing run. The simulation includes physically motivated and phenomenologically supported multiband and VHE emission from a structured jet in the afterglow phase, as well as a full modeling of the CTAO instrument response to the expected time-variable spectral energy distributions, as described in the following sections. The events are further processed through a realistic scheduling framework that takes account of their visibility from both the southern and northern CTAO arrays in operational darkness conditions, along with an appropriate observing strategy. These consist of multiple consecutive observations, called tiling, which are strategically selected to provide coverage of a large fraction of the GW uncertainty region.

This paper is organized as follows. In Section 2, we describe the sample of simulated BNS systems and the associated GW signals that we use in this work. In Section 3, we detail how we simulated the VHE emission associated with BNS mergers. In Section 4, we describe the characteristics of CTAO. In Sections 5 and 6, we present the simulations of the CTAO follow-up of BNS mergers and propose observational strategies to optimize the probability of detection of EM counterparts to GW events. Finally, in Section 7 we describe and discuss our results, and in Section 8 we present our conclusions.

## 2. Simulated GW Events from BNS Mergers

The realistic ensemble of simulated BNS mergers and the associated GW signals presented in P. Petrov et al. (2022), which has been released publicly on Zenodo (L. Singer 2021), is used in these simulations. This BNS sample, consisting of 2307 events, defines the size of our full GW–GRB simulation set, since each BNS has been connected to a GRB emission (see Section 3.) The sample has been built considering realistic astrophysical distributions of masses, spins, distances, and sky locations. Specifically, the NS component masses were randomly extracted from a normal distribution with mean 1.33 $M_{\odot}$ and standard deviation 0.09 $M_{\odot}$, consistent with that inferred from measurements related to binary systems in the Galaxy (F. Özel & P. Freire 2016). The NS spins are aligned or antialigned, with uniformly distributed magnitudes smaller than 0.05: the maximum allowed value is consistent with the spin of the most rapidly rotating pulsar found in a binary system, i.e., PSR J0737-3039A (M. Burgay et al. 2003). The position and the orientation of the binaries are distributed isotropically, and the redshifts are drawn uniformly in comoving rate density, employing cosmological parameters from Planck Collaboration et al. (2016). For each BNS merger, the expected GW inspiral signal has been simulated and then convolved with the GW detector responses, considering different GW detector network configurations. For this work, we select the simulations performed assuming a network composed by Advanced LIGO, Advanced Virgo, and KAGRA, with the sensitivities expected to be reached in the fifth LVK observing run (O5), whose timeline is consistent with the one of CTAO; these sensitivities have been released in B. O'Reilly et al. (2020). The obtained BNS simulations have then been analyzed with the matched-filtering technique (L. A. Wainstein & V. D. Zubakov 1962; K. Cannon et al. 2012; T. Dal Canton et al. 2014; J. Veitch et al. 2015; T. Adams et al. 2016; S. A. Usman et al. 2016; C. Messick et al. 2017; A. H. Nitz et al. 2017), assuming a 70% independent duty cycle for each interferometer. The signals are considered as GW candidates if they are detected with a network signal-to-noise ratio above 8, even if observed with a single interferometer: this approach has been shown to be representative of the public GW alerts sent during the third LVK observing run (O3) (P. Petrov et al. 2022). Finally, for each GW simulated candidate, the associated sky localization has been estimated with BAYESTAR, which is a rapid Bayesian position reconstruction code that computes source location using the output from the detection pipelines (L. P. Singer et al. 2014). Included in this localization information is the 90% credible region (CR) skymap, utilized in all observation strategies and presented in Section 6.

## 3. Estimation of the VHE Emission from Phenomenological Prescriptions

The estimate of the VHE emission is performed by adopting a simple, phenomenological model. All BNS merger events included in the simulated catalog (see Section 2) are assumed to successfully launch a relativistic collimated outflow (i.e., jet), whose energy dissipation leads to emission of radiation known as short GRB. This hypothesis is adopted for simplicity because considerations of the uncertainties in jet launching mechanism and propagation lie beyond the scope of this work. Yet, only a fraction of events may be capable of launching a jet that successfully penetrates the ejecta and achieves a breakout (A. Colombo et al. 2022; O. S. Salafia et al. 2022a; N. Sarin et al. 2022), which is subject to discussion in Section 7.

Based on the information available for each simulated GW event (and in particular distance and viewing angle $\theta_{\rm view}$, defined as the angle between the jet axis and the line of sight to the observer), the jet-related emission in the CTAO energy range is estimated from phenomenological prescriptions based on the currently available observations of short GRBs at different wavelengths and on the current knowledge of VHE emission from GRBs. The adopted approach does not require the specific population of particles or the specific radiative mechanism responsible for the production of gamma rays. Since we are interested in long-lasting radiation, we focus on VHE emission produced in the context of the interactions between the jet and the surrounding medium, i.e., afterglow radiation.

The information currently available from GRBs at VHE includes: (i) five detections of long GRBs either by MAGIC (MAGIC Collaboration et al. 2019a; H. Abe et al. 2024), H.E.S.S. (H. Abdalla et al. 2019; H. E. S. S. Collaboration et al. 2021), or LHAASO (LHAASO Collaboration et al. 2023); (ii) one hint of emission from a short GRB by MAGIC (V. A. Acciari et al. 2021); and (iii) flux upper limits inferred from observations of a large number of (mostly long) GRBs by MAGIC, H.E.S.S., and HAWC (F. Aharonian et al. 2009; A. Albert et al. 2022; S. Abe et al. 2025b).

Past detections of long GRBs between 0.1 and 10 TeV have shown that the luminosity emitted in this energy range is comparable to the luminosity emitted in the soft X-ray band

(MAGIC Collaboration et al. 2019b; L. Nava 2021; D. Miceli & L. Nava 2022) and decays in time at a similar rate (H. E. S. S. Collaboration et al. 2021). Given a current lack of observational evidence of short GRBs at TeV energies, we assume here that TeV radiation in short GRBs behaves in the same way, i.e., that its TeV luminosity is comparable to the X-ray one and decays at a similar rate. If this assumption is not proven by future observations, part of the results in this paper might require substantial revision.

Spectra of the VHE detected GRBs are consistent with a photon index around $\alpha = -2$ (in the notation $dN/dE \propto E^{\alpha}$, where $dN/dE$ is the number of photons per unit of energy), ranging from $-1.6$ (H. Abdalla et al. 2019, although poorly constrained) to $-2.5$ or even softer, depending on time and the extragalactic background light (EBL) model (MAGIC Collaboration et al. 2019a; Z. Cao et al. 2023). Since the sample of detected GRBs is still very limited, interesting information can come also from observed GRBs with no evidence of VHE excess. In these cases, the flux upper limits can be estimated and compared with the properties of VHE detected GRBs.

Starting from these pieces of information, we predict VHE afterglow light curves and spectra for an observer located at an angle $\theta_{\rm view}$ from the jet axis. This requires a jet structure to be specified, i.e., a description of how the kinetic energy density and Lorentz factor of the jet depend on the angle $\theta$ from the jet axis.

In the next sections, we specify all the assumptions on the adopted parameters and give the details of the method that has been applied to simulate the light curves and spectra of VHE radiation.

### 3.1. Jet Properties and Structure

We consider a jet with a Gaussian structure in energy and bulk Lorentz factor (B. Zhang & P. Mészáros 2002; P. Kumar & J. Granot 2003)

$$\epsilon_{\rm k}(\theta) = \epsilon_{\rm k,core}\, e^{\left(-\frac{\theta^2}{\theta^2_{\rm core}}\right)} \quad (1)$$

$$\Gamma_0(\theta) = (\Gamma_{0,\rm core} - 1)\, e^{\left(-\frac{\theta^2}{2\theta^2_{\rm core}}\right)} + 1. \quad (2)$$

Here, $\theta$ is the angle from the jet axis and ranges from $\theta = 0^\circ$ and $\theta = \theta_{\rm MAX}$, where $\theta_{\rm MAX}$ is defined as the minimum between $90^\circ$ and the angle that verifies the condition $\Gamma_0(\theta_{\rm MAX}) = 5$. This condition is introduced to limit the computation time (see similar approaches in G. Ryan et al. 2020; C. Pellouin & F. Daigne 2024). The energy per unit solid angle of the core is $\epsilon_{\rm k,core} \sim E_{\rm k,core}/\pi\theta^2_{\rm core}$. Hence, the jet's structure depends on three quantities: the opening angle $\theta_{\rm core}$, the initial Lorentz factor $\Gamma_{0,\rm core}$, and the core kinetic energy $E_{\rm k,core}$. The value of $\theta_{\rm core}$ is randomly assigned according to the distribution based on the few estimates inferred from the population of short GRBs seen on axis. We use a lognormal distribution with $\langle {\rm Log}(\theta_{\rm core}/{\rm deg})\rangle = 1.15$ (corresponding to $14^\circ$) and $\sigma_{{\rm Log}\theta_{\rm core}} = 0.2$ (W. Fong et al. 2015). Lacking a statistical study of bulk Lorentz factors in short GRB jets, its value has been randomly assigned from a lognormal distribution peaked at $\Gamma_{0,\rm core} = 200$ (a value similar to the bulk Lorentz factor adopted to model emission from GRB 170817A (G. Ghirlanda et al. 2019; O. S. Salafia et al. 2019) and standard deviation $\sigma = 0.2$.

The kinetic energy of the jet $E_{\rm k,core}$ at the beginning of the afterglow emission is derived from the gamma-ray energy emitted during the prompt phase by assuming an efficiency $\eta_\gamma$ for the prompt emission: $E_{\rm k,core} \sim E_\gamma\,(1-\eta_\gamma)/\eta_\gamma$. Note that the initial jet energy can be computed as $E_{0,\rm jet} = E_\gamma/\eta_\gamma$. The collimation corrected energy $E_\gamma$ is related to the more commonly used isotropic equivalent energy $E_{\gamma,\rm iso}$: $E_\gamma \sim E_{\gamma,\rm iso}\,(1-\cos\theta_{\rm core})/2$. We associate to each event an energy $E_{\gamma,\rm iso}$ according to considerations reported in the next section.

### 3.2. $E_{\gamma,iso}$ Distribution

$E_{\gamma,\rm iso}$ is defined as the isotropic equivalent energy emitted in the prompt phase as inferred by an on-axis observer (i.e., an observer whose line of sight lies within the jet's core). The $E_{\gamma,\rm iso}$ distribution for the population of short GRBs is built based on the population study presented in G. Ghirlanda et al. (2016).

Following G. Ghirlanda et al. (2016), we first assign to each event a peak energy $E_{\rm peak}$, randomly extracted from the distribution given in their Equation (13). For the values of the function parameters, we adopt the mode values for model *a* reported in their Table 1. In this case, the $E_{\rm peak}$ distribution is described by

$$\phi(E_{\rm peak}) \propto \begin{cases} \left(\frac{E_{\rm peak}}{1.4\ {\rm MeV}}\right)^{-0.8} & \text{for } 0.1\ {\rm keV} < E_{\rm peak} < 1.4\ {\rm MeV} \\ \left(\frac{E_{\rm peak}}{1.4\ {\rm MeV}}\right)^{-2.6} & \text{for } 1.4\ {\rm MeV} < E_{\rm peak} < 100\ {\rm MeV} \end{cases}. \quad (3)$$

For a given value of $E_{\rm peak}$, the associated value of $E_{\gamma,\rm iso}$ is calculated using the Amati correlation for short GRBs reported in G. Ghirlanda et al. (2016) (Equation (15), with parameters taken from model (a), Table 1, mode values)

$$\log_{10}(E_{\gamma,\rm iso}/10^{51}\,{\rm erg}) = 0.036 + 1.1\,\log_{10}(E_{\rm peak}/670\,{\rm keV}). \quad (4)$$

Once $E_{\gamma,\rm iso}$ has been assigned, the collimation corrected prompt energy $E_\gamma$, the kinetic energy of the jet after the prompt emission $E_{\rm k,core}$, and the initial jet energy $E_{0,\rm jet}$ can be computed (see the previous section). Their distributions are shown in the inset of Figure 1, where a value of $\eta_\gamma = 0.2$ has been assumed for the radiative efficiency.

As a consistency check, we estimate the efficiency in converting the mass of the disrupted NS into the energy of the jet, $\eta_{\rm jet} \equiv E_{0,\rm jet}/M_{\rm low}c^2$. The distribution of this quantity is shown in Figure 1, for which we note the agreement with the typical expected values (O. S. Salafia & B. Giacomazzo 2021; A. Colombo et al. 2025).

### 3.3. VHE Light Curves and Spectra

To reproduce the range of spectral behaviors observed in VHE detected GRBs, photon indices are extracted from a Gaussian distribution peaked at $\alpha = -2.2$ and with standard deviation $\sigma = 0.1$.

To build the VHE light curves, we base our method on the similarity between VHE and soft X-ray afterglow light curves. As shown in several studies (Y. Kaneko et al. 2007; P. D'Avanzo et al. 2012; R. Margutti et al. 2013), the luminosity of the X-ray afterglow (typically estimated in the band 0.3–10 keV) correlates with $E_{\gamma,\rm iso}$, and this is observed both in long and short GRBs. In most cases, this correlation is studied with reference to the X-ray luminosity measured at 11 hr. Adopting the relation for short GRBs found by E. Berger (2014)

$$L_{\rm X,11\,hr} = 8.5 \times 10^{43} E^{0.83}_{\gamma,\rm iso,51}\ {\rm erg\ s^{-1}}, \quad (5)$$

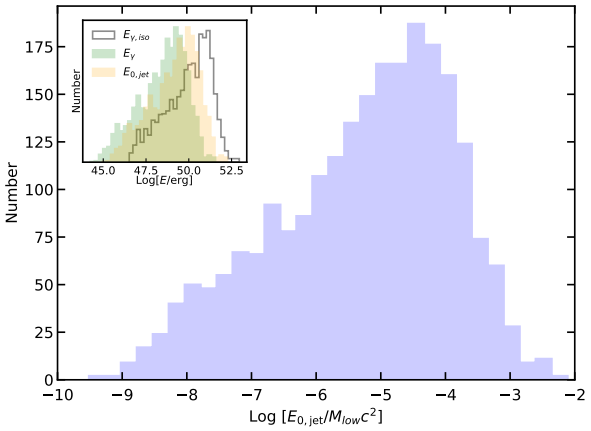


**Figure 1.** Ratio between the energy of the jet launched following the merger of the BNS and the mass of the lightest NS. The inset shows the distributions of the jet energy $E_{0,\rm jet}$ (orange filled histogram), the radiated energy $E_\gamma$ (green filled histogram), and the isotropic equivalent radiated energy $E_{\gamma,\rm iso}$ (black empty histogram).

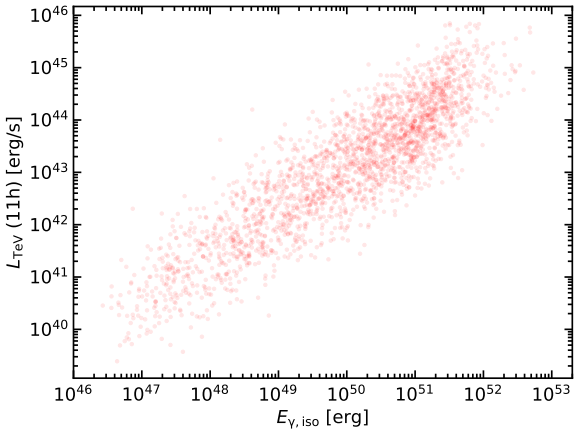


**Figure 2.** TeV luminosity at 11 hr versus $E_{\gamma,\rm iso}$ for the sample of short GRBs simulated in this work.

we estimate $L_{\rm X,11\ hr}$ from $E_{\gamma,\rm iso}$. To account for the observed dispersion around the best fit line, we consider a Gaussian scatter of half an order of magnitude.

Based on the observation that for long GRBs the X-ray and VHE luminosities are similar, the VHE luminosity at 11 hr ($L_{\rm TeV,11\ hr}$) integrated in the energy range 0.3−1 TeV of our sample of simulated short GRB afterglows is computed assuming that the ratio $L_{\rm TeV,11\ hr}/L_{\rm X,11\ hr}$ has a lognormal distribution peaked at 0 and with standard deviation $\sigma = 0.3$. The resulting correlation between $L_{\rm TeV,11\ hr}$ and $E_{\gamma,\rm iso}$ is shown in Figure 2. The scatter plots of $L_{\rm TeV,11\ hr}$ and $L_{\rm X,11\ hr}$ together with their distributions are shown in Figure 14.

To build the rest of the VHE light curve, we proceed as follows. We assume that the luminosity increases as a power-law $L_{\rm TeV} \propto t^{\beta_1}$ up to the deceleration time, when it reaches its maximum. The value of $\beta_1$ is randomly extracted from a Gaussian distribution with $\langle\beta_1\rangle = 2$ and $\sigma_{\beta 1} = 0.05$ (LHAASO Collaboration et al. 2023). The deceleration radius is computed as

$$R_{\rm dec}(\theta) = \left(\frac{17\,E_{\rm k}(\theta)}{16\,\pi\,m_{\rm p}c^2\,n\,\Gamma_0^2(\theta)}\right)^{\frac{1}{3}} \quad (6)$$

where the density of the external medium $n$ is assumed to be constant and equal to 0.1 particle cm$^{-3}$.

After the peak, during the deceleration, the luminosity decreases as $L_{\rm TeV} \propto t^{\beta_2}$. The value of $\beta_2$ is assigned after the assumption that VHE and X-ray light curves decay at a similar rate, in analogy with what broadly observed in long GRBs. We collected a sample of 22 short GRBs and fit their light curves with a power-law function (see Appendix). The distribution of temporal decay indices is well described by a Gaussian function with mean value $\langle\beta_2\rangle = -1.45$ and $\sigma_{\beta 1} = 0.48$. The temporal decays of VHE light curves after the peak are randomly extracted from this distribution. At this point, the VHE light curve for an observer oriented along the jet axis is known.

### 3.4. Computation of the Off-axis Emission

The emission received by an observer located at an angle $\theta_{\rm view}$ is estimated following the method proposed in G. P. Lamb & S. Kobayashi (2017). Each differential element of the jet is identified by spherical coordinates ($\theta$ and $\phi$), with the jet axis located at $\theta = 0°$. For each jet element, the evolution of the bulk Lorentz factor is assumed to be constant before the deceleration radius (see Equation (6)) and to decrease in time after the deceleration (R. D. Blandford & C. F. McKee 1976)

$$\Gamma(R,\,\theta) = \begin{cases} \Gamma_0(\theta) & \text{for } R < R_{\rm dec}(\theta) \\ \left(\frac{17\,E_{\rm k}(\theta)}{16\,\pi\,m_{\rm p}\,n_0\,c^2\,R^3}\right)^{\frac{1}{2}} & \text{for } R > R_{\rm dec}(\theta) \end{cases}. \quad (7)$$

Following G. P. Lamb & S. Kobayashi (2017), first we estimate the flux received at each observer time by an on-axis observer and then apply corrections to estimate the contribution of each element to the observer located at $\theta_{\rm view}$. Finally, the emission received by the observer is obtained at each time by integrating over all the contributions from different elements of the jet arriving at the same time.

A randomly selected sample of simulated light curves is shown in Figure 3. The figure illustrates that the GRB viewing angle has a dual effect on the gamma-ray light curves, shifting them toward both lower spectral fluxes and later times after the sGRB onset. This emphasizes the viewing angle as a key parameter influencing the detectability of an sGRB event. The flux is highest when the observer lies within the opening angle of the jet core, i.e., when the ratio $\theta_{\rm view}/\theta_{\rm core} < 1$, as shown in Figure 3 (right panel). Comparing the light curves with the average CTAO-South sensitivity further highlights the role of the viewing angle in determining the detectability of a given event.

## 4. The Cherenkov Telescope Array Observatory in Time-domain Astronomy

CTAO is the next-generation ground-based gamma-ray observatory and is currently under construction. It will be composed of two arrays of IACTs, one located in the northern hemisphere (CTAO-North, Observatorio Roque de los Muchachos, La Palma, Spain), and one in the southern hemisphere (CTAO-South, Paranal, Chile), which together will provide full sky coverage. The arrays consist of a different combination of telescope designs, which will guarantee a wide energy coverage: the design of CTAO-North includes a total of four large size telescopes (LSTs; optimized for the 20 GeV–1 TeV energy

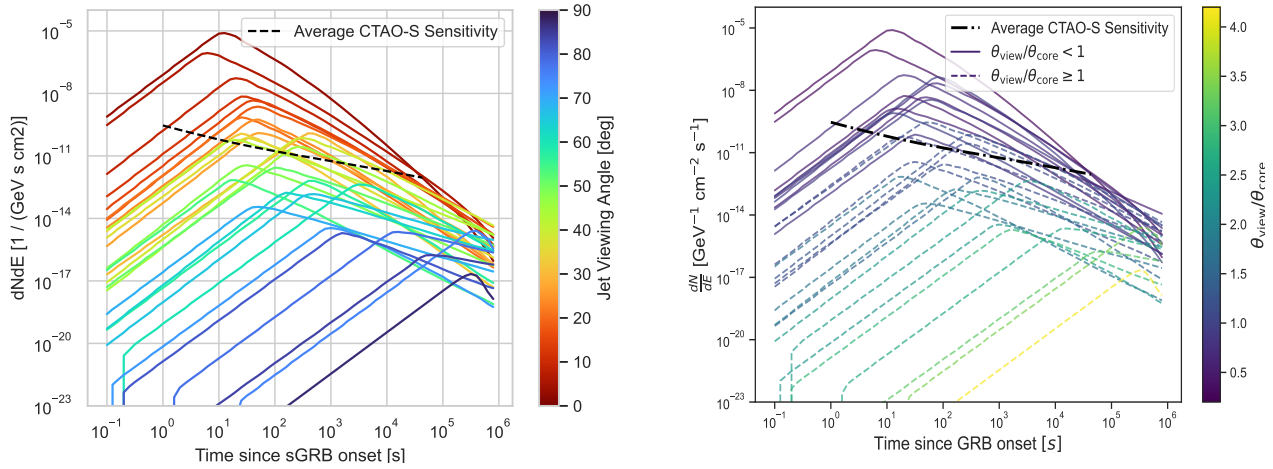


**Figure 3.** Subset of sGRB light curves at 100 GeV generated using the procedure described in Section 3. Left panel: The color scale corresponds to the off-axis viewing angle between jet and observer, $\theta_{view}$. The dashed black line indicates the average sGRB integral flux sensitivity of the CTAO-South Alpha Configuration (see Section 4), for an exposure time equal to the scale of the $x$-axis. Right panel: Subsample of GRB light curves color coded by their respective ratio of $\theta_{view}/\theta_{core}$. Events for which $\theta_{view}/\theta_{core} > 1$ are shown with dashed lines. The CTAO-South sensitivity is shown for comparison, calculated using the average spectral shape of events in the subsample.

range) and nine medium size telescopes (MSTs, optimized for the 100 GeV–50 TeV energy range), while CTAO-South will consist of 14 MSTs and 37 small size telescopes (SSTs, optimized for the 1 TeV–300 TeV energy range). This configuration is named the "Alpha Configuration."

CTAO will play a crucial role in gamma-ray astronomy due to its unprecedented sensitivity, up to an order of magnitude better than current instruments, its rapid slewing capabilities (e.g., the LSTs can be repointed in about 20 s), its large FoV ranging from 4.3° to 10° depending on the telescope, and angular resolution (down to few arcminutes) (Cherenkov Telescope Array Consortium et al. 2019). In addition, CTAO will have a very high sensitivity to short-timescale phenomena: at energies above few tens of GeV, it offers $10^4$–$10^5$ better sensitivity than the LAT instrument onboard the Fermi satellite for the detection of short-duration transient phenomena (S. Funk et al. 2013; see also https://www.ctao.org/for-scientists/performance/).

### 4.1. The Ingestion of GW Alerts with CTAO

CTAO features the array control and data acquisition (ACADA) system (I. Oya et al. 2024), which coordinates telescope operations, data acquisition, and real-time data processing, executing prescheduled observations and those triggered by science alerts. Science alerts can be triggered externally (e.g., through GCN or VoEvent), or internally thanks to the science alert generation (SAG) pipeline (A. Bulgarelli et al. 2022), which processes incoming Cherenkov data, reconstructs events, and generates science alerts within 20–30 s at nominal CTAO sensitivity.

External and internal alerts are ingested by the transient handler (TH), a subsystem of ACADA (K. Egberts et al. 2022). The TH validates the alerts, applies configurable science filters, and, when warranted, triggers, updates, or retracts follow-up observations.

In the context of responding to GW alerts, the TH will play a central role in validating and selecting the numerous alerts expected during O5 and in implementing the optimal observation strategy. This includes selecting the ensemble of observation coordinates required to cover to cover a significant localization region, scheduling observing times, and configuring subgroups of telescopes (i.e., subarrays) to maximize scientific output within the constraints of the GW alerts and based on current knowledge of the expected gamma-ray counterparts. More details will be provided in Section 6.

Furthermore, the SAG enables the evaluation of acquired data for early identification of transient phenomena and the generation of internal candidate scientific alerts, submitted to the TH. To this end, and because sky area is tiled with multiple pointings, data stacking across multiple observations is essential. In cases involving large sky regions, the system developed by ACADA ensures accurate stacking over consistent coordinates throughout the entire observation campaign, even in the presence of observing gaps.

### 4.2. CTAO Telescopes Configuration and Instrument Response Function

The performance characterization of the CTAO is based on detailed Monte Carlo simulations, leading to the generation of instrument response functions (IRFs). These IRFs quantify the sensitivity, effective area, angular and energy resolution, and background rates of the array as functions of energy, observation direction, and offset angle.

The current baseline layout adopted for CTAO is known as the Alpha Configuration and was described in the previous subsection. The IRFs associated with this configuration were derived from the Prod5 simulations (Cherenkov Telescope Array Observatory & Cherenkov Telescope Array Consortium 2021). These use CORSIKA (v7.7) and sim-telarray toolchains, incorporating updated models of atmospheric properties, telescope optics, and electronics (Cherenkov Telescope Array Observatory & Cherenkov Telescope Array Consortium 2021), and represents a substantial advancement over previous simulation sets. Because performance is heavily dependent on pointing, the Prod5 IRFs contain performance estimates for both the northern and southern arrays at three different zenith angles: 20°, 40°, and 60°. The lower energy thresholds adopted for each zenith are $E_{min}$ used in this work are 20 GeV, 32 GeV, and 130 GeV, respectively. The maximum energy $E_{max}$ adopted is 10 TeV for all IRFs.

## 5. Simulation of CTAO Observation and Analysis

The VHE emission derived in the previous sections is used as the input emission for which the CTAO detectability prospects are evaluated. We include the attenuation of the intrinsic GRB spectrum by the EBL, as modeled in A. Franceschini & G. Rodighiero (2017), to obtain the observed flux for each GRB. For the simulation of the CTAO response, the CTAO Alpha Configuration is considered, as described in Section 4.

In these simulations, the exposure time required for CTAO to detect each event is estimated as a function of the delay time from the onset of the GRB emission. This approach allows for the evaluation of each GRB's detectability within the parameter space defined by exposure time and delay. The minimum fluence detectable by CTAO is computed using the IRFs (see Section 4) and the exposure time is calculated as the time required for a $5\sigma$ detection by CTAO. All significance values and detection criteria in the following sections refer to pretrial significance, unless stated otherwise.

### 5.1. Simulating CTAO Response to BNS Merger Events

The following step in our pipeline is to simulate the response of CTAO to each of the GRB events produced as described in Section 3. The ultimate goal of these simulations is to find, for each event, the functional relationship between latency from the onset of the merger and the total observation time needed to achieve a $5\sigma$ detection level with CTAO. Given this relationship, one can quickly perform a lookup to check how much observation time is needed to detect an event given the current latency. This analysis yields several insights, including the average detectability rate across all simulated events and the influence of GRB and jet properties on detectability. In addition, these results can be provided as input to help optimize real observing strategies (see Section 6).

Observations of the correct source position typically start after a certain latency $t_L$ from the BNS merger time $t_0$: $t_{\rm start} = t_0 + t_L$. $t_L$ has contributions from many stacking factors, including the time for the LVK collaboration to process and emit a GW alert, as well as the TH handling and the telescope slewing time. In addition, a number of different pointings may be necessary before the true source location is pinpointed, each of which contributes to $t_L$.

The strategy for calculating this relationship relies on comparing the flux needed to detect the EM counterpart at a $5\sigma$ level with CTAO, $F_{5\sigma}^{\rm CTAO}$, with the average flux of the source $F_{\rm avg}$. The time needed for detection $t_{\rm det}$ is defined as the exposure time ($t_{\rm exp}$) that satisfies the following equality:

$$F_{\rm avg}(t_{\rm exp};\, t_L) = F_{5\sigma}^{\rm CTAO}(t_{\rm exp}). \tag{8}$$

The average flux is given by

$$F_{\rm avg}(t_{\rm exp};\, t_L) = \frac{S(t_{\rm exp};\, t_L)}{t_{\rm exp}} \tag{9}$$

where $S$ is the intrinsic source fluence:

$$S(t_{\rm exp};\, t_L) = \int_{t_L}^{t_L + t_{\rm exp}} \int_{E_{\rm min}}^{E_{\rm max}} \phi(E,\, t)\, E\, dE\, dt \tag{10}$$

where $\phi(E,\, t)$ represents the GRB spectra as described in Section 3, and $E_{\rm min}$ and $E_{\rm max}$ correspond to the energy limits of the CTAO IRFs (Section 4). In the above equations, we assume that the GRB onset time is simultaneous with BNS merger time, such that we can explicitly set $t_0 = 0$.

These simulations are performed with a custom-tailored Python package called `sensipy` (J. G. Green et al. 2026), which takes CTAO IRFs, an EBL model (A. Franceschini & G. Rodighiero 2017), and GRB simulations as input and calculates detection times given a variety of initial conditions and user inputs, essentially by solving Equation (8). For the management of spectral models, the package depends on primitives from `gammapy`, the analysis package used by CTAO (A. Donath et al. 2023).

### 5.2. CTAO Response to Simulated GRBs

We begin with the simulated CTAO response to the 2307 GW–GRB events to estimate the impact of observing time on $5\sigma$ detectability. Each GRB is simulated with six different CTAO IRFs: both sites, and at three different zenith angles (20°, 40°, and 60°). In addition, each event is observed with each IRF at 50 different $t_L$, distributed on a logarithmic scale from 10 s to 7 days, leading to a total catalog size of nearly $7 \times 10^5$ simulations. Figure 4 shows the average relationship between $t_L$ and $t_{\rm det}$ only for events that are detectable by CTAO within 7 days of the GRB onset, about ∼16% of the total sample. These curves show how the average exposure time needed for a $5\sigma$ detection increases with the increasing time delay between the GW–GRB onset and the start of observations at the true source location. In the same figure, we also show the fraction of events detectable with the average exposure time at the given latency. As expected, the fraction of detectable events decreases with increasing latency. In addition, with a latency lower than ∼1 hr, the exposure time necessary for detection remains more or less constant. Similarly, the fraction of detected events also decreases after a similar latency time. Finally, in comparing the results for on- and off-axis sub-samples at low latencies, on-axis GRBs can be detected within a few minutes on average, whereas off-axis GRBs require ∼10 minutes for detection. Above this same threshold of ∼1 hr, the viewing angle of the event becomes much less important and the detection timescales exponentially with the latency for all events. These results emphasize the fact that, as observed for long GRB, the first minutes to hours are critical for detecting GW–GRB coincidences (H. Abdalla et al. 2019; MAGIC Collaboration et al. 2019a; H. E. S. S. Collaboration et al. 2021; H. Abe et al. 2024).

Another way to interpret these simulations is to consider a specific value of $t_L$ or $t_{\rm exp}$, and estimate the probability of detecting a certain event. As a concrete example, a GW-follow-up scheduler must make an informed decision when no signal is detected yet: keep observing the same position or move on to the next pointing? Figures 5(a) and (b) illustrate that, in most cases, significantly increasing the exposure time does not increase the chances of detection. Extending an observation from 1 to 20 minutes only increases the overall probability of detection from 10.3% to 14%. In addition, Figures 5(c) and (d) indicate that latencies longer than a few hours significantly decrease the probability of detection. In most cases, continuing observations beyond ∼6 hr presents a significant challenge for joint detections. The large difference in detectability between on-axis and off-axis events is driven by the connection between spectral flux and $\theta_{view}$, as noted in Figure 3. In addition, we observe that observations with a latency of 24 hr may still be fruitful. Overall, the plots in

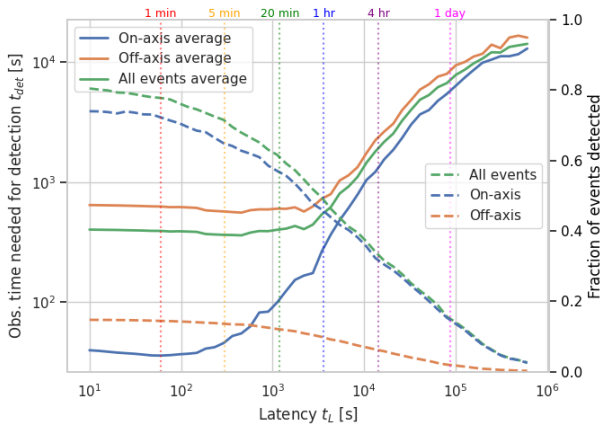


**Figure 4.** All curves in this plot are calculated using only events which are detectable by CTAO within 7 days of GRB onset. For these detectable events, the solid curves show the average observation time needed to reach the $5\sigma$ significance threshold given a latency $t_L$ between GW onset and start of observations. For observing latencies of $t_L \lesssim 1$ hr, nearly the entire population of detectable GRBs can be detected with observations of 1–10 minutes exposures. After this threshold, the viewing angle of the GRB is not an important contributing factor to the observation time needed for detection. The dashed curves show the fraction of events which are detectable given $t_L$. Once again, after the 1 hr threshold, the fraction of detections descends from a constant 20% to nearly 0% after 24 hr. All curves show the relative importance of the first few hours post-trigger.

Figure 5 suggest that, under the assumption that the simulated population of BNS mergers well represents the true distribution, on-axis events offer a significant opportunity for a joint detection with CTAO.

In order to obtain a more holistic view of the $t_L$-$t_{\rm exp}$ parameter space, in Figure 6 we plot both variables together against the fraction of detected events in the sample. Here, we define a new parameter that represents the effective viewing angle of the source $\theta_{\rm eff} = \theta_{\rm view} - \theta_{\rm core}$, where $\theta_{\rm view}$ is the viewing angle of the observer. When $\theta_{\rm eff} < 0$, the observer is on axis and therefore subject to viewing the beaming effect of the GRB jet, whereas off-axis events are defined by $\theta_{\rm eff} > 0$, dominating our population of GW–GRBs, being 87% of the total population.

Two distinct regions of detectability are visible, separated by a steep curve in latency space. For both on- and off-axis GRBs, the detectability exhibits a pronounced decline for an observational latency of approximately 1 hr, with the precise latency threshold at which this decrease occurs being dependent of the exposure. These heatmaps also show that for $t_L = 10$ minutes, approximately 67% of on-axis sources can be detected with an exposure time of $\leqslant$1 minute. For a longer latency of $t_L = 1$ hr, the fraction of detected events is 47% with the same exposure time of $\leqslant$1 minute. For off-axis events, these rates go down to 11% and 7% for $t_L = 10$ minutes and $t_L = 1$ hr, respectively. It can also be seen that detections are only slightly more likely at CTAO-South compared to CTAO-North, which we interpret as resulting from the larger number of MSTs. We obtained an overall detection rate of 18.3% and 17.6%, respectively. Finally, contour lines on these heatmaps indicate a potential strategy for IACT follow-up campaigns: pick a constant value of probability from such heatmaps and use these to calculate the exposure time at each pointing. It is also important to note that these numbers do not yet take into account day and night cycles, the moon, and other observational limits which would affect the true detectability of a given source. These factors will be considered in Section 6.

### 5.3. Linking CTAO Response to GW–GRB Parameters

Given the large sample of events simulated under different observing conditions and values of $t_L$, we can also examine the relationship between the inherent parameters of the simulated GRBs with the CTAO response. The corner plot of Figure 7 explores the relationship between various observational parameters and detectability. The parameters considered include source distance $d$, isotropic energy $E_{\rm iso}$, the angular size of the 90% CR of the GW skymap, the opening angle of the GRB jet $\theta_{\rm core}$, the effective viewing angle $\theta_{\rm eff}$ (see Section 5.2), and the latency $t_L$.

The corner plot indicates that both $\theta_{\rm eff}$ and $t_L$ have the most distinct populations between detected and undetected events of the sample. While $t_L$ is always known during follow-up campaigns, GW observatories do not currently provide any estimate on $\theta_{\rm view}$ (B. P. Abbott et al. 2020). Should they gain such an ability to provide constraints on the orientation of mergers with respect to the observer, this could provide one of the most stringent criteria for whether to carry out a GW follow-up.

## 6. Observing Strategies

Compared to other transient sources, GW follow-up observations present an extra level of complexity given the average extension of the source localization uncertainty region. During O4, tens of GW candidates have been localized down to several (tens of) degrees for their 50% (90%) CR, e.g., S250119cv (Ligo Scientific Collaboration et al. 2025a) or S241102br (Ligo Scientific Collaboration et al. 2025b), see GraceDB[190] for the full list. These uncertainty regions can be further reduced as more GW interferometers join the global network and contribute to the GW sky localization. The LST and MST telescopes of CTAO are designed to cover a large fraction of the VHE energy range where we expect most of the GRBs above-GeV emission. The FoV of these telescopes, with $\rm FoV_{radius} \sim 2.5$ deg, means that GW events with a 90% CR smaller than $\sim$20 deg$^2$ may be subsequently observed as point-like sources, following a wobble strategy. Anything larger than this will require a dedicated follow-up strategy.

### 6.1. Tiling Observations of Poorly Localized GWs

A substantial number of GW detections will exhibit poorly constrained localization, highlighting the importance of observation strategies. Following up such poorly localized events presents a particular challenge for pointing instruments such as CTAO, which require robust localization strategies. In this work, the observation campaign for each GW is handled by `tilepy` (M. Seglar-Arroyo et al. 2024), which is a software package designed to plan and optimize follow-up observations of transient events with extended sky localizations. It ingests probabilistic sky localization maps (e.g., HEALPix maps from the LVK network) and generates candidate telescope pointings based on the instrument FoV, site visibility, and observational constraints. This tool optimizes the selection and scheduling of these pointings to

[190] gracedb.ligo.org/superevents/S240615dg

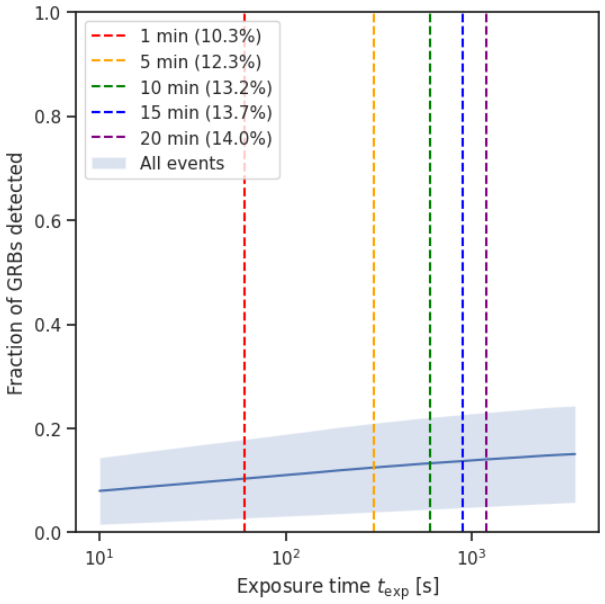


(a) Fraction of all events detected with increasing exposure time

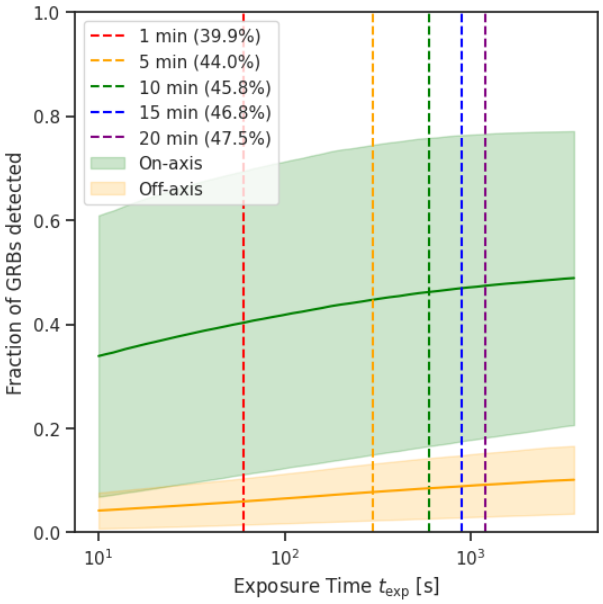


(b) Fraction of on- and off-axis events detected with increasing exposure time

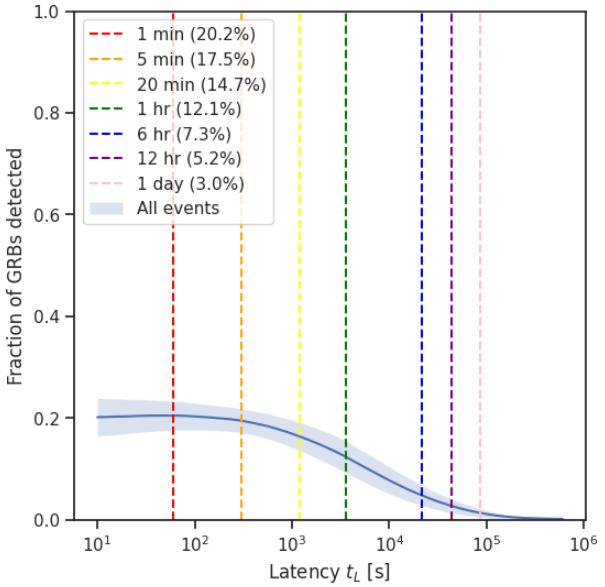


(c) Fraction of all events detected with increasing latency after GRB onset

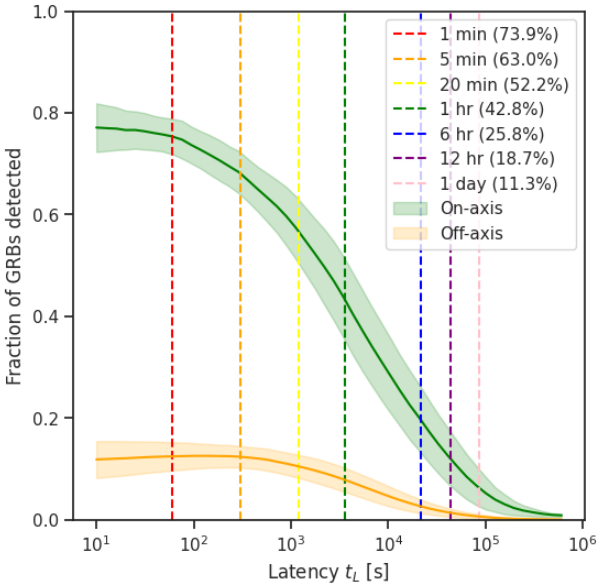


(d) Fraction of on- and off-axis events detected with increasing latency after GRB onset

**Figure 5.** These curves explore the relationship between the fraction of events detected and two follow-up observation parameters: exposure time on source position $t_{exp}$ and latency time after coalescence $t_L$. The upper left and right panels show how increasing exposure leads to a cumulative increase in detections, for all events and on- and off-axis events, respectively. In all cases, increasing exposures beyond $t_{exp} \gtrsim 10$ minutes leads to only a small increase in the fraction of detected events from the sample. The lower panels show how increasing $t_L$ for all, on-, and off-axis events lead to a vanishing fraction of detectable GRBs. On average, the fraction of detected events decreases fourfold after latencies of $\sim$12 hr. In this sample, each event is simulated 300 times, at different values of zenith, CTAO site, and with $t_L$ ranging from 10 s to 7 days. The large uncertainty bands around some curves are due to small samples sizes of detectable events.

maximize the covered localization probability while accounting for latency, exposure time, night duration, and observing conditions such as zenith angle. In this study, we focus on the temporal observation campaign optimization by studying how this choice impacts the GRB detectability results. For this purpose, we have identified three different scenarios regarding exposures: fixed exposures, average GRB emission exposures, and adaptive exposures.

The first case studied focuses on fixed observation exposures. We have selected three different exposures, which account to a total of three different cases. These are: 1 minute exposure time (to study the fastest case, for which from Section 5 the source is detected in $\sim$73% of the on-axis cases and $\sim$12% of the off-axis cases); a 5 minute exposure time, for which the source is detected in $\sim$63% of the on-axis cases ($\sim$12% of the off-axis); and 20 minute exposure time, for

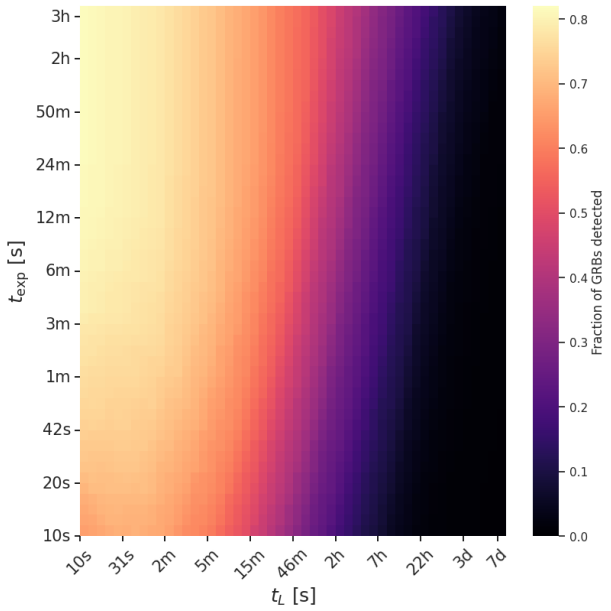


(a) CTAO-South on-axis

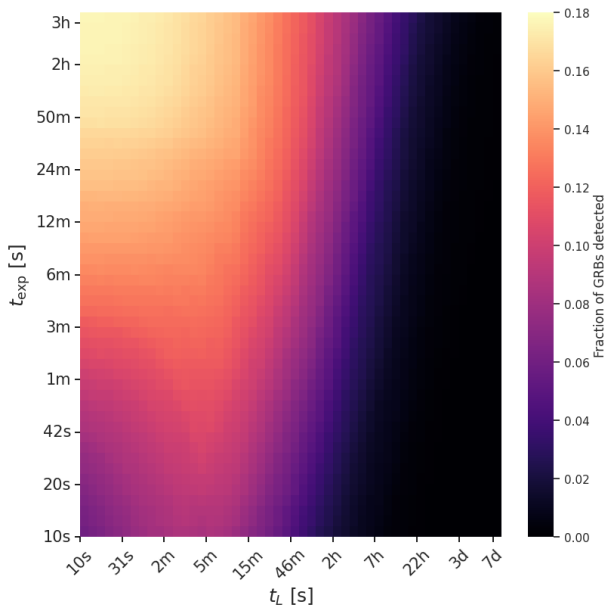


(b) CTAO-South off-axis

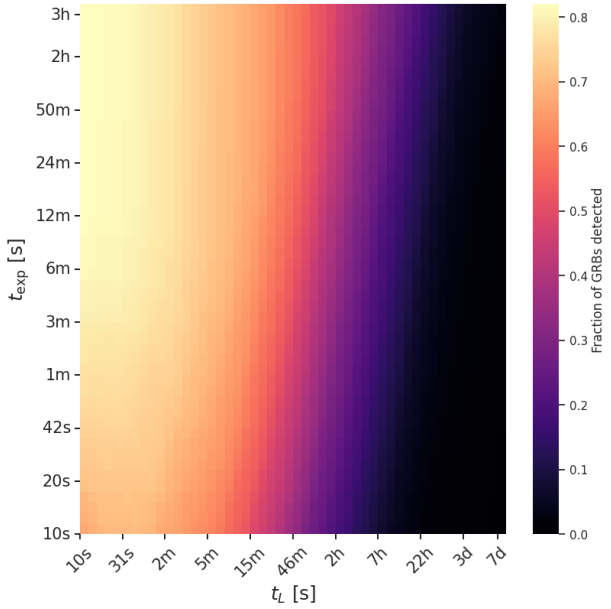


(c) CTAO-North on-axis

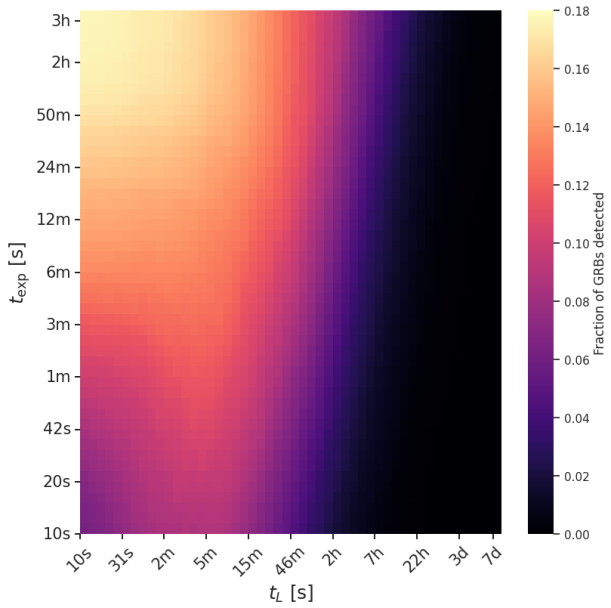


(d) CTAO-North off-axis

**Figure 6.** Detectability heatmaps for short GRBs using CTAO-South (upper row) and CTAO-North (bottom row) across the complete simulated dataset, shown as functions of latency $t_L$ and exposure time $t_{exp}$. The left column displays results restricted to on-axis sources with viewing angles within the opening angle of the jet (namely having $\theta_{eff} < 0$), whereas the right column encompasses all sources within $\theta_{eff} > 0$. The color scale represents the proportion of simulated events successfully detected, with brighter tones indicating enhanced detection efficiency. Notably, we note that the largest detectability change due to the observation latency appears between 1–4 hr, which ultimately depends on the observation exposure.

which the source is still detected in ∼52% of the on-axis cases (∼10% of the off-axis). Note that the latest choice coincides with the standard pointing duration in current generation IACTs, and is therefore adopted in most VHE follow-up campaigns.

The second case concerns exposures modulated according to the temporal evolution of an average GRB emission, derived from the full set of light curves in our sample, which generates a sort of representative source. For every new pointing, we calculate the time necessary to achieve a $5\sigma$ detection of this representative source, incorporating the pointing latency $t_L$ (following Equation (8)). Crucially, we now treat the exposure time per tiling, typically a static configuration parameter, as an adjustable degree of freedom, necessitating specific adaptations within `tilepy`.

Finally, in our third study scenario, we incorporate the known spectral evolution of each GRB when scheduling its pointings. While such a strategy cannot be used during real follow-ups, it can provide a baseline for the efficiency of a campaign. Within this framework, the exact exposure time for

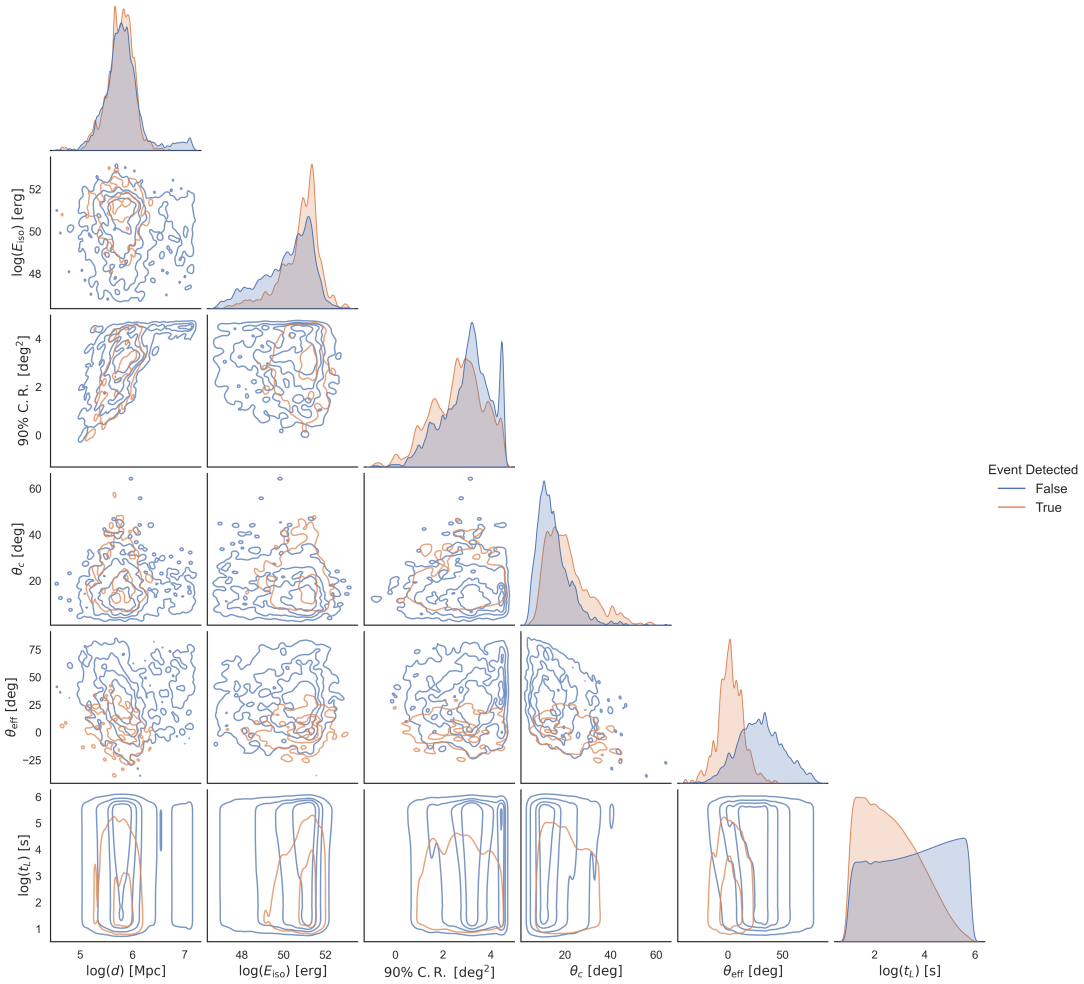


**Figure 7.** Relationship between pairs of intrinsic GRB and observational parameters. Blue points represent detectable events from our sample while orange points are nondetectable events. $\theta_{\rm core}$ is the opening angle of the cone of the GRB jet and $\theta_{\rm eff}$ is the angular distance between the observer and the edge of the cone. The strongest distinction between the distributions of detectable and nondetectable events seen in $\theta_{\rm eff}$ suggests that the single most important factor contributing to detectability is whether or not the observer lies within or near the edge of the jet. In addition, we see once more that with latencies $t_L$ under a few hours, we have a higher number of simulated events which are detectable.

each pointing is determined as the period necessary to achieve a $5\sigma$ signal, accounting for each event's specific light curve and the current latency $t_L$, as described in Section 3. This stringent requirement ensures, by definition, that the source is always detected, provided that the tiling successfully encompasses its position within the observing constraints. We note that for some events, however, this strategy can lead to large delays before source position coverage, especially compared to the short, fixed-window strategies.

We ran `tilepy` on the full set of GW–sGRB simulations for the three mentioned scenarios, which account for a total of five configurations. In all cases, a conservative FoV radius of $2.^{\circ}5$ is selected for the scheduling, corresponding to the radius at which the camera acceptance has decreased by a factor $\sim$2. This value is intended to be representative of an overall combined FoV of CTAO. The simulation is configured to have a maximum duration of three full days. The selected observation windows are realistic. We consider the site visibility conditions, which include Sun position, Moon position (for which we allow for observations under certain moonlight conditions defined by altitude, phase and separation to the observation coordinates), and the evolution of the localization region throughout the night. First, we note that, for all cases, the observability conditions at the observatory represent a key consideration that modulates the CTAO's duty cycle and these results. These considerations are taken into account to assess the scheduling of the source for the input merger time of the BNS and the GRB evolution. The detectability of a GRB depends on the zenith angle of the observation, which changes the energy threshold and effective area. The precision of the current study is set by the available IRFs, which are derived for fixed zenith angle values of 20°, 40°, and 60° (see Section 4). These are used in our study to obtain the $5\sigma$ signal condition evaluated for each possible tiling after a preselection based on the probability coverage. For a pointing to be scheduled, its coordinates must be observable by the telescope at both the beginning and end of the proposed window; otherwise the pointing is skipped. This process is repeated until the full observing campaign is assembled. The future CTAO will produce tailored Monte Carlo simulations for the analysis of the acquired data, which will improve the detection prospects of our tiling strategy.

This approach folds the duty cycle of IACTs in our simulation chain, which reaches $\sim$15% per site over a year, including day time.

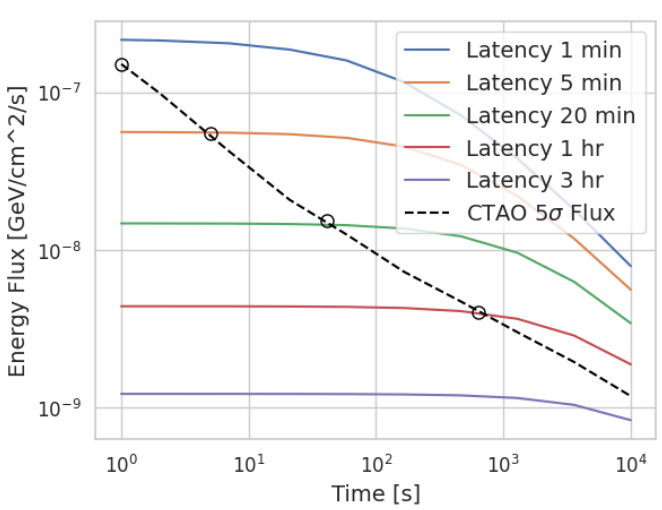


(a) Example GRB lightcurves for one event at different latencies (colored lines). The intersection of these curves with the $5\sigma$ CTAO Flux sensitivity (dashed line) indicates the observation time needed to achieve a detection for each latency. For the lightcurves, the horizontal axis represents time since GRB onset, while for the sensitivity curve it represents observation time $t_{\rm exp}$.

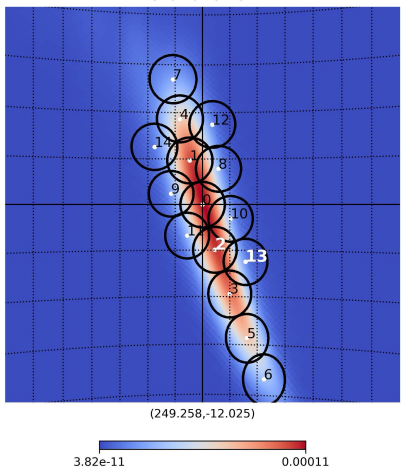


(b) Observation scheduling for the GW skymap associated to the example GW-GRB event. The color scale represents the probability region provided by the interferometer pipeline, and the numbers indicate the sequential ordering of CTAO observations. The source is detected both in pointings 2 and 13, indicated by white numbers.

**Figure 8.** Example light curves and tiling strategy for a representative event from the sample. This sGRB is seen on axis, has an $E_{\rm iso} = 1.21 \times 10^{51}$ erg, and it is located at a distance $d = 991$ Mpc. The EBL is taken into consideration with the models from A. Franceschini & G. Rodighiero (2017). The resulting skymap has a 90% credible area of 345 deg$^2$.

An example of the integration between tiling, CTAO sensitivity, and the GRB light curves can be found in Figure 8.

The results of the five configurations are shown in Figure 9. The total probability covered versus the total exposure time is presented, with their distributions projected for the horizontal and vertical dimensions. We identify the characteristics of the various scheduling simulations. In purely scheduling terms, the fixed-duration campaigns, i.e., the 1', 5', and 20' minute campaigns, show how we can cover a large CR with a very limited number of observations. Then, the average observation campaign scenario is not able to cover a large GW localization uncertainty region. This effect is driven by the off-axis GRB subsample, which requires long exposure times at low latencies, being sub-optimal in realistic scenarios where no detailed information on the GRB emission is available beforehand. Similarly, a relatively low number of pointings are scheduled in the adaptive campaign because many dimmer off-axis GRBs do not meet the detectability requirement for scheduling.

Tiled observations can also contain a certain degree of sky overlap, enabling the coverage of some sky regions multiple times. Figure 10 shows the number of times that the coordinates of the injected GW–GRB simulation are covered in each approach. In the absence of information about the energetics and temporal evolution of the GW–GRB source, short individual observations enable repeated coverage of the source location. In the most extreme case, i.e., 1 minute campaigns, the source can be revisited up to several tens of times, particularly for well-localized events. In Figure 10, we observe that the tested adaptive campaigns, including average- and variable-window campaigns, also produce such scenarios, i.e., the selected windows coincide with the fixed-duration

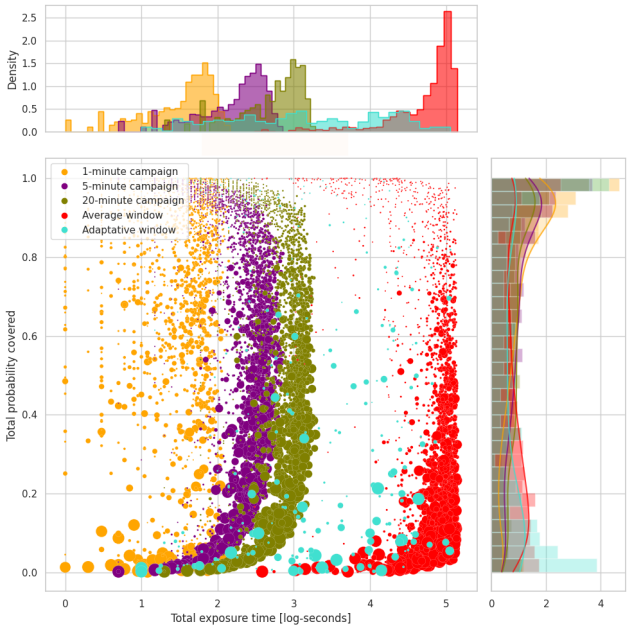


**Figure 9.** Total GW location uncertainty (named probability for simplicity) covered in terms of the total exposure time for the five configurations explored in this work. The size of the markers corresponds to the size of the GW uncertainty regions, depicted for qualitative considerations.

short window results. These cases correspond to well-localized events in combination with favorable energetics.

### 6.2. Detection Rates for Follow-up Strategies

Just because a source location is covered quickly or with many repeated tilings does not imply that the event will be

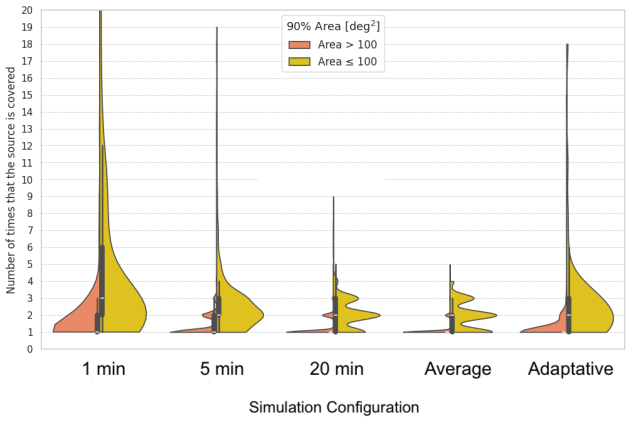


**Figure 10.** Distribution of the number of times that the GW–GRB source location is covered during the follow-up observation campaign of CTAO for the different strategies presented in this work.

detected. In order to fully evaluate the performance of the various scheduling algorithms, the tiling strategies must be folded with the detectability of each source. The results on the number of detected events versus follow-up campaign duration are shown in Figure 11, where the number of detectable o n-axis and off-axis GRBs is shown. Across all strategies, increasing the duration of follow-up campaigns beyond $\sim$3 $-$4 hr provides rapidly diminishing benefits in terms of the number of events detected. When looking at off-axis GRBs only, this threshold decreases to $\sim$1 hr. This indicates that a follow-up campaign duration of $\sim$4 hr would be optimal to balance detection probability with telescope time used.

Table 1 highlights summary statistics comparing each of the proposed campaign strategies, indicating that all three fixed-window campaigns manage to cover between 60%–70% of all followed-up events. With a fixed 4 hr follow-up, 4.5%$-$5.1% of events are consistently detected regardless of the chosen strategy. However, the shorter 1 and 5 minute campaigns tend to produce higher detection significances because the faster tiling provides a greater chance to reach the source position sooner or even cover it multiple times.

### 6.3. The Role of the Science Alert Generation

We can further evaluate the performance of each strategy by considering how the internal self-triggering alerts are produced by the SAG. Specifically, we focus on the real-time analysis (RTA). The RTA pipeline reconstructs the gamma-ray direction and energy from signals detected in the telescope cameras. It then generates and analyzes sky images in real time, concurrently assessing the detectability of observed sources over time. For dedicated GW–GRB campaigns, an RTA system strategically optimized for rapid response is essential. Such a system would identify signal hot spots within the telescope's FoV, allowing for an immediate cessation of the tiling schedule and a focused reallocation of observational resources to the detected hotspot.

Figure 12 shows the distribution of accumulated significance for a fixed-duration campaign with RTA, indicating that with RTA $\sim$4% ($\sim$2%) of total events can be detected at $\geqslant 10\sigma$ ($\geqslant 100\sigma$), regardless of the chosen strategy.

Upon revisiting Table 1, we can also note the crucial role of the RTA in increasing the statistics of GRB detections beyond the $5\sigma$ threshold. Fixing the remaining campaign time at the correct position doubles the detection significance on average and increases it by more than tenfold in some cases. In addition, the amount of observation time used to directly observe the source position increases by 2–3 orders of magnitude. The importance of RTA cannot be overstated because the extra time directly leads to better resolved spectra, the possibility for detailed light curves, and higher statistics at energies near the CTAO threshold.

## 7. Discussion on Joint Rates Estimates

The feasibility of joint detections of GW and sGRBs by the LVK and CTAO is estimated to be around 4%–5%. This joint detection rate is contingent upon several hypotheses, particularly the BNS merger rate and the successful jet fraction of GRBs, both parameters carrying considerable uncertainty.

### 7.1. Impact of the Uncertainties on CBC Populations

The joint detection rates of GW–GRB events depend on the BNS merger rate. P. Petrov et al. (2022) referred to the published observational rate density estimates from the third LVK GW transient catalog (GWTC-3): $R_{\rm BNS}^{\rm GWTC3} = 10 - 1700\ {\rm Gpc}^{-3}\ {\rm yr}^{-1}$, as 90% credible interval obtained by combining the rates estimated from different population models (R. Abbott et al. 2023). The most recent value, constrained including results from the first part of the fourth LVK observing run (O4a) and reported in the fourth LVK transient catalog (GWTC-4) is instead $R_{\rm BNS}^{\rm GWTC4} = 7.6 - 250\ {\rm Gpc}^{-3}\ {\rm yr}^{-1}$; also in this case, the numbers refer to the 90% credible interval obtained by combining the rates estimated from different population models (The LIGO Scientific Collaboration et al. 2025). In both R. Abbott et al. (2023) and The LIGO Scientific Collaboration et al. (2025), the impact of the population model selection and systematics are outlined, which yields to differences in the predicted BNS rates of various orders of magnitude. If we consider the number of BNSs in P. Petrov et al. (2022) used in this work, we expect to observe during observing run O5 $190^{+410}_{-130}$ BNS mergers per year, based on recent updates of the expected duration and sensitivity of the O5 observing run. The BNS simulations used in this work are compared with those provided by the International Gravitational Wave Network (IGWN), which are used in the latest released BNS rates using GWTC-3 (R. W. Kiendrebeogo et al. 2023). In this later work, the considerations on the populations that yield to CBCs include a continuous mass distribution across the various CBC subpopulations (i.e., the three populations from the combinations of pairs of neutron stars and black holes), instead of a truncated Gaussian distribution per subpopulation. In the comparison, we find that the annual number of detected BNSs during O5 doubles (R. W. Kiendrebeogo et al. 2023, $180^{+220}_{-100}$, P. Petrov et al. 2022, $86^{+171}_{-9}$). More recently, O. S. Salafia (2025) presented the detection probability of BNS in O5 with a simplified approach that is independent of the uncertain mass distribution of the merging binaries and which uses only the information on the past number of detections, combined with an estimate of the ratio between the sensitivity of the target run with respect to the previous runs. Based on this study, the number of BNSs we expect to observe in O5 is $28^{+44}_{-21}$. Thus, we conclude that the uncertainties regarding future BNS detections, which include the LVK network sensitivity and the CBC populations, are an important part of the systematic errors affecting our detection prospects. Regarding the localization uncertainty regions, the median 90% CR source localization obtained in

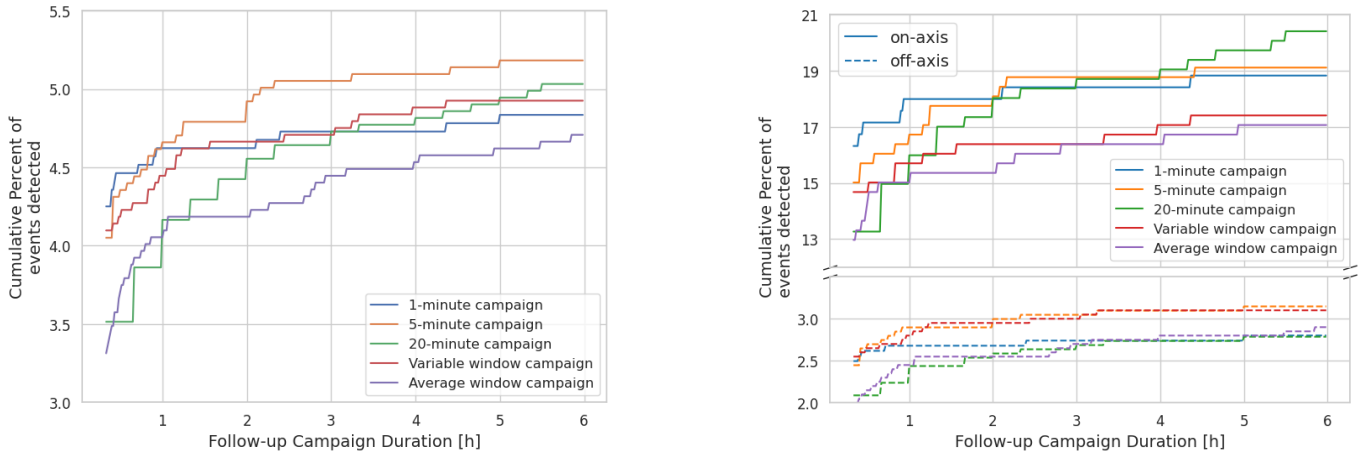


(a) All events (b) On- and off-axis events

**Figure 11.** Evolution of detection rates with increasing duration of follow-up campaign starting from the time when the first pointing is possible. An event can reach a $5\sigma$ detection in one single pointing or when the cumulative significance of multiple correct pointings reaches the same threshold. The left panel compares the cumulative percentage of detected events for five different follow-up strategies and shows that, overall, after 3–4 hr the effectiveness of the variable, 1, and 5 minute campaigns stagnate. The right panel shows the on- and off-axis detection rates for the same strategies, each normalized to the number of events in their respective sample. Notably, for off-axis events, little seemed to be gained after following any strategy beyond ∼1 hr.

P. Petrov et al. (2022) and R. W. Kiendrebeogo et al. (2023) barely changes, from which we conclude that the findings of the observation strategies presented in this work will remain unaffected. Future GW detections will lead to tighter constraints on the BNS merger rate, thereby enhancing the precision of the prospects outlined in this work.

### 7.2. Impact of the Uncertainties on Very-high-energy Gamma Rays from GRBs

All of the scenarios considered in this work assume successful VHE emission resulting from beamed afterglow radiation characteristic of jetted GRBs. Yet, the fraction of BNS mergers producing jetted GRBs remains uncertain. Recent studies estimate that between 20% and 50% of the entire BNS population may be able to produce a jet (N. Sarin et al. 2022; O. S. Salafia & G. Ghirlanda 2022).

In addition, we do not expect this scenario to apply universally. BNS mergers may instead produce choked jets—i.e., jets that fail to successfully breakout—such as was initially proposed for GW170817 during the first week after the merger, before VLBI observations confirmed the presence of a launched jet. Looking ahead, gamma-ray observations will play a critical role in constraining emission models, thereby refining our understanding of jet formation and geometry in these events. The LST-1 observations on the BOAT GRB 221009 have highlighted the capability of gamma-ray measurement to place stringent constraints on jet models, including from late times observations (K. Abe et al. 2025a) .

### 7.3. The Role of the Observing Strategies in IACTs

Observation strategies are designed to align with the specific goals of each campaign and can be guided by either prior hypotheses about the source or by agnostic data-driven considerations. In this work, we explore both approaches. For poorly localized transient events with low occurrence rates, the chosen strategy is particularly critical, although it is often complicated by limited knowledge of individual GRB sources and the GRB population. Our primary objective is to strike a balance between search sensitivity and sky coverage within a fixed maximum observing window.

In addition, there is the possibility that telescopes may split into multiple subarrays that scan different regions of the sky in parallel. As shown in M. Seglar-Arroyo et al. (2024), this multitelescope strategy (or divergent pointing mode) is especially powerful in the case of large telescope arrays such as CTAO, since the coverage at time $t_{\rm cov}^{N}$ scales as $t_{\rm cov}^{N} \sim 1/N \cdot t_1$ ($N$: number of telescopes, $t_1$: time to cover a region by a single telescope), modulated by the effective FoV of the subset of telescopes selected. This improvement comes at the expense of decreasing the sensitivity of the observation given smaller arrays, although the largest improvement in sensitivity due to strong background rejection arises in the transition from single-telescope to stereoscopic observations. While modifying the scheduling workflow for the N-observatory case is not in the scope of this paper, we acknowledge that subarray strategies will be key for effective follow-up campaigns of poorly localized transient events.

Finally, we highlight that galaxy catalogs were not incorporated into the observational strategy discussed herein. These catalogs are standard tools in GW follow-up campaigns and are crucial for optimizing sky coverage by precisely identifying probable host galaxies, a methodology successfully demonstrated in the case of GW170817 (B. P. Abbott et al. 2017b). While a comprehensive evaluation of the benefits of integrating galaxy catalogs is beyond the purview of this study, we nevertheless acknowledge their considerable potential to augment detection efficiency. This potential is intrinsically linked to ongoing improvements in the completeness of galaxy catalogs, such as the GLADE+ catalog (G. Dálya et al. 2022), the DESI Legacy Imaging Surveys (A. Dey et al. 2019), or the catalogs that will be produced with the Vera Rubin Observatory,[191] which promise deeper and more comprehensive coverage of potential host galaxies.

[191] https://www.lsst.org/about/dm/data-products

**Table 1**
Summary Statistics for Each of the Five Follow-up Campaign Scenarios

| | 1 Minute | 5 Minute | 20 Minute | Variable | Average |
|---|---|---|---|---|---|
| Percent (%) | | | | | |
| Percent covered | 70.0 | 65.9 | 62.9 | 6.7 | 44.7 |
| Percent detected [4 hr campaign] | 4.7 | 5.1 | 4.8 | 4.9 | 4.5 |
| Time (minute) | | | | | |
| Mean time until source position reached | 136.3 | 186.5 | 260.6 | 158.0 | 217.1 |
| Mean source duration [no RTA, 4 hr campaign] | 0.6 | 1.7 | 4.4 | 0.3 | 2.5 |
| Mean source duration [RTA, 4 hr campaign] | 204.7 | 193.0 | 184.1 | 204.6 | 197.5 |
| Significance ($\sigma$) | | | | | |
| Median sig. [no RTA, 4 hr campaign] | 29.2 | 22.5 | 8.3 | 11.2 | 19.9 |
| Median sig. [RTA, 4 hr campaign] | 91.4 | 49.3 | 43.1 | 83.7 | 58.5 |

**Note.** Coverage refers to whether the source position was successfully covered at least once by the scheduler. Source duration refers to the amount of time observing the correct source position. Finally, in scenarios with a robust real-time analysis (RTA) system, the scheduler can stop its scanning campaign and observe the correct source position as soon as a $5\sigma$ detection has been reached.

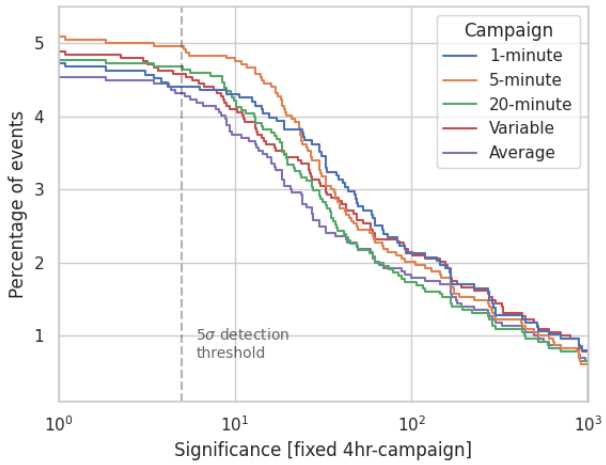


**Figure 12.** Distribution of the accumulated significance, displaying the detection and characterization capabilities of CTAO for the GW–GRB sample when the SAG system is involved, given a fixed 4 hr follow-up campaign with each strategy. In all cases, a SAG-RTA system was simulated, which stops the scheduler once a $5\sigma$ hotspot is detected in the FoV and self-triggers observations of the source for the remaining duration of the campaign.

## 8. Summary

In this work, we have explored the prospects of joint detection of GW by LVK during observing run O5 and sGRB detections by CTAO, for which the emission has been estimated from phenomenological descriptions and the latest simulated CTAO IRFs (Alpha Configuration). We evaluated the role of observation strategies and how these can modulate the chance of detecting EM counterparts to GWs, especially in poorly localized events. We highlighted the role of RTA in enabling the self triggering of observations, improving the significance of detections, which in turn will enable an in-depth study of astrophysical sources, such as the sGRBs evaluated here. The observational and macrophysical parameters used in our study can be constrained in the case of nondetection at VHE energies.

The full simulation chain of short GRBs associated with GW events, referred to as GW–GRBs, shows that approximately 18% of the GW–GRB sample emits VHE gamma-ray radiation detectable by CTAO. This fraction is largely driven by off-axis events, which dominate the GW–GRB population, with on-axis events being detectable in a much higher fraction (see Section 6). When detectability is combined with effective observability, accounting for realistic scheduling and observatory visibility, follow-up, and tiling strategies, a set of useful prescriptions for future CTAO observational planning emerges. Notably, follow-up campaigns in regions of large GW localization uncertainty become significantly less effective beyond 1–4 hr after the event, with minimal gains in detected events for longer observation times.

Our analysis reveals that observation strategies based on either fixed or variable tile durations do not present significant variations, with the spread in detectable event percentages across strategies remaining within 25%. Intriguingly, the highest number of detected sources is achieved with 5 minute observations, reaching a 5.1% detection rate with a fixed 4 hr campaign. Although shorter 1 minute exposure times facilitate faster source acquisition, they exhibit a distinct performance difference compared to 20 minute observations, consistent with theoretical predictions. Therefore, we conclude that a 5 minute strategy represents an effective trade-off, balancing the requirements for exposure time and spatial coverage necessary for source detection.

The implementation of RTA is crucial for integrating signals from significant hot spots, thereby increasing the scientific information that can be extracted from each event. Similarly, we can infer that longer observation times for well-localized events can provide valuable constraints, even in the absence of a detection.

The key macrophysical parameters influencing detectability are the jet opening angle and the viewing angle. In this regard, obtaining even rough estimates of the viewing angle in GW alerts would enable CTAO to prioritize the most promising events, maximizing detection prospects and also constraining the physical parameters of the GW–GRB system.

We note that the strategies discussed here do not incorporate other potentially useful information, such as the distribution of galaxies within the GW uncertainty region—an element that was crucial in the localization of GRB 170817. This highlights that there is still room for improvement in the observational strategies, which will be explored in future work.

We have assessed how the results presented in this work rely on the various assumptions made concerning observations, astrophysical populations and rates, and gamma-ray

emission, so that changes on these can be easily incorporated into the predicted fractions of detectable events.

The full simulation chain described here, developed within the CTAO Consortium, will be employed in forthcoming studies to further characterize the physical conditions that give rise to VHE emission and to assess the impact of CTAO observations in constraining the TeV GW–GRB population and the environment of BNS mergers. This work can also be extended to explore other populations, such as neutron star–black hole (NSBH) mergers, and to consider future GW interferometers, including the Einstein Telescope. For these next-generation instruments, a careful definition of selection criteria will be crucial to identify GW events of potential interest amid the large number of detections expected.

## Acknowledgments

*CTAO consortium acknowledgments*. We gratefully acknowledge financial support from the following agencies and organizations:

State Committee of Science of Armenia, Armenia; The Australian Research Council, Astronomy Australia Ltd, The University of Adelaide, Australian National University, Monash University, The University of New South Wales, The University of Sydney, and the Western Sydney University, Australia; Federal Ministry of Education, Science and Research, and Innsbruck University, Austria; Conselho Nacional de Desenvolvimento Científico e Tecnológico (CNPq), Fundação de Amparo à Pesquisa do Estado do Rio de Janeiro (FAPERJ), Fundação de Amparo à Pesquisa do Estado de São Paulo (FAPESP), Fundação de Apoio à Ciência, Tecnologia e Inovação do Paraná—Fundação Araucária, and the Ministry of Science, Technology, Innovations and Communications (MCTIC), Brasil; Ministry of Education and Science, National RI Roadmap Project DO1-153/28.08.2018, Bulgaria; The Natural Sciences and Engineering Research Council of Canada and the Canadian Space Agency, Canada; ANID PIA/APOYO AFB230003, ANID-Chile Basal grant FB 210003, Núcleo Milenio TITANs (NCN19-058), FONDECYT-Chile grants 1201582, 1210131, 1230345, and 1240904; Croatian Science Foundation, Rudjer Boskovic Institute, University of Osijek, University of Rijeka, University of Split, Faculty of Electrical Engineering, Mechanical Engineering and Naval Architecture, University of Zagreb, and the Faculty of Electrical Engineering and Computing, Croatia; Ministry of Education, Youth and Sports, MEYS LM2018105, LM2023047, EU/MEYS CZ.02.1.01/0.0/0.0/16_013/0001403, CZ.02.1.01/0.0/0.0/18_046/0016007, CZ.02.1.01/0.0/0.0/16_019/0000754, and CZ.02.01.01/00/22_008/0004632, Czech Republic; Academy of Finland (grant nr.317636 and 320045), Finland; Ministry of Higher Education and Research, CNRS-INSU and CNRS-IN2P3, CEA-Irfu, ANR, Regional Council Ile de France, Labex ENIGMASS, OCEVU, OSUG2020 and P2IO, France; The German Bundesministerium für Forschung, Technologie und Raumfahrt (BMFTR), the Max Planck Society, the Deutsche Forschungsgemeinschaft (DFG, with Collaborative Research Centre 1491), and the Helmholtz Association, Germany; Department of Atomic Energy, Department of Science and Technology, India; Istituto Nazionale di Astrofisica (INAF), Istituto Nazionale di Fisica Nucleare (INFN), MIUR, and Istituto Nazionale di Astrofisica (INAF-OABRERA) Grant Fondazione Cariplo/Regione Lombardia ID 2014-1980/RST_ERC, Italy; ICRR, University of Tokyo, JSPS, and MEXT, Japan; Netherlands Research School for Astronomy (NOVA) and the Netherlands Organization for Scientific Research (NWO), Netherlands; University of Oslo, Norway; Ministry of Science and Higher Education, DIR/WK/2017/12, the National Centre for Research and Development and the National Science Centre, UMO-2016/22/M/ST9/00583, Poland; Slovenian Research and Innovation Agency, grants P1-0031, I0-E018, J1-60014, Slovenia; South African Department of Science and Technology and National Research Foundation through the South African Gamma-Ray Astronomy Programme, South Africa; the Spanish groups acknowledge funds from "ERDF A way of making Europe," the Spanish Ministry of Science, Innovation and Universities, and the Spanish Research State Agency (AEI) via MCIN/AEI/10.13039/501100011033, grants CNS2023-144504, PDC2023-145839-I00, PID2022-137810NB-C22, PID2022-139117NB-C41/C42/C43/C44, PID2022-136828NB-C41/C42, PID2022-138172NB-C41/C42/C43, PID2021-124581OB-I00, PID2021-125331NB-I00, and budget lines 28.06.000X.411.01 and 28.06.000X.711.04 of PGE 2023, 2024 and 2025; the "Centro de Excelencia Severo Ochoa" program through grants no. CEX2019-000920-S, CEX2020-001007-S, CEX2021-001131-S; the "Unidad de Excelencia María de Maeztu" program through grants no. CEX2019-000918-M and CEX2020-001058-M; the "Ramón y Cajal" program through grant RYC2021-032991-I; and the "Juan de la Cierva" program through grants no. JDC2022-048916-I and JDC2022-049705-I. We also acknowledge the projects with refs. PR47/21 TAU and TEC-2024/TEC-182, both funded by the Comunidad de Madrid regional government. Funds were also granted by the "Consejería de Universidad, Investigación e Innovación" of the regional government of Andalucía (Refs. AST22_00001_9 and AST22_0001_16) and "Plan Andaluz de Investigación, Desarrollo e Innovación" (Ref. FQM-322); and by the "Programa Operativo de Crecimiento Inteligente" FEDER 2014-2020 (Refs. ESFRI-2017-IAC-12 and ESFRI-2020-01-IAC-12) and Spanish Ministry of Science, Innovation and Universities, 15% co-financed by "Consejería de Economía, Industria, Comercio y Conocimiento" of the Gobierno de Canarias regional government. The Generalitat de Catalunya regional government is also gratefully acknowledged via its "CERCA" program and grants 2021SGR 00426 and 2021SGR 00679. The Spanish groups were also kindly supported by European Union funds via the Horizon Europe Research and innovation program under Grant Agreement no. 101131928; NextGenerationEU, grants no. PRTR-C17.I1, CT19/23-INVM-109, and the "MicroStars" ERC, ref. 101076533. This research used computing and storage resources provided by the Port d'Informació Científica (PIC) data center; Swedish Research Council, Royal Physiographic Society of Lund, Royal Swedish Academy of Sciences, The Swedish National Infrastructure for Computing (SNIC) at Lunarc (Lund), Sweden; State Secretariat for Education, Research and Innovation (SERI) and Swiss National Science Foundation (SNSF), Switzerland; The National Research Foundation of Ukraine (project 2023.03/0149 and 2023.05/0024), Ukraine; Durham University, Leverhulme Trust, Liverpool University, University of Leicester, University of Oxford, Royal Society, and the Science and Technology Facilities Council, UK; U.S. National Science Foundation, U.S. Department of Energy, Argonne National Laboratory, Barnard College, University of California, University of Chicago, Columbia University, Georgia Institute of Technology, Institute for Nuclear and Particle Astrophysics (INPAC-MRPI program), Iowa State

University, the Smithsonian Institution, V.V.D. is funded by NSF grant AST-1911061, Washington University McDonnell Center for the Space Sciences, and The University of Wisconsin and the Wisconsin Alumni Research Foundation, USA. The research leading to these results has received funding from the European Union's Seventh Framework Programme (FP7/2007–2013) under grant agreements No 262053 and No 317446. This project is receiving funding from the European Union's Horizon 2020 research and innovation programs under agreement No 676134.

F. Schüssler acknowledges ANR (French National Research Agency) for its support of the project "Multimessenger Observations of the Transient Sky (MOTS)" under grant No. ANR-22-CE31-0012.

A. Colombo and A. Stamerra acknowledge partial financial support by Italian Research Center on High Performance Computing Big Data and Quantum Computing (ICSC), project funded by European Union—NextGenerationEU—and National Recovery and Resilience Plan (NRRP)—Mission 4 Component 2 within the activities of Spoke 2 (Fundamental Research and Space Economy), (CN 00000013 - CUP C53C22000350006)

A. Stamerra acknowledges financial support from INAF through the "Ricerca Fondamentale 2024" on the GO/GTO program titled "Discovering the New TeV Frontier of Gravitational Wave Counterparts through Follow-up Observations with the MAGIC Telescopes."

L. Nava acknowledges financial support from the European Union-Next Generation EU, PRIN 2022 RFF M4C21.1 (202298J7KT - PEACE)

*Software:* Astropy (Astropy Collaboration et al. 2013, 2018; Astropy Collaboration, et al. 2022), gammapy (A. Donath et al. 2023), Sensipy (J. G. Green et al. 2026), tilepy (M. Seglar-Arroyo et al. 2024).

## Author Contributions

This publication is the result of a collaborative effort within the CTAO Consortium, developing an integrated simulation framework connecting gravitational-wave detections, short gamma-ray burst emission models, and CTAO response simulations to assess the observatory's capability to detect very-high-energy counterparts of compact binary mergers. The project was coordinated by A. Stamerra, who supervised its development, guided the scientific discussion, and oversaw the manuscript preparation. L. Nava led the simulation of the intrinsic and time-dependent spectra of short gamma-ray bursts and their VHE emission, providing the phenomenological assumptions used in the study. B. Patricelli implemented and adapted the simulations of gravitational-wave–detected binary neutron star systems and contributed to the subsequent CTAO observation simulations. J. Green led the development of the dedicated package `sensipy` for simulating CTAO observations, carried out the analysis, and produced associated results and figures. M. Seglar-Arroyo implemented the observing strategies within `tilepy`, generated the tiled observations used to scan the gravitational-wave skymaps, and produced the figures. F. Schüssler led the `tilepy` development and contributed to the scientific discussions. All the authors participated in the interpretation of the results, preparation of the manuscript, and editing.

The rest of the authors have contributed in one or several ways to the development of the CTAO analysis tools and IRFs and participated in the review of the manuscript through internal discussions and approval processes coordinated by the Transients Working Group leaders and the CTAO Speakers and Publications Office (CTAO-SAPO). The initial manuscript drafts were reviewed by E. Bissaldi, F. Longo, and I. Agudo on behalf of CTAO-SAPO. All of the above authors have participated in the paper discussion and edition.

## Appendix
## Derivation of Temporal Decays of VHE Light Curves and X-Ray and TeV Luminosities

To derive the temporal decay index $\beta_2$ of the VHE light curves during the deceleration phase, it is assumed that they follow the same distribution as the X-ray light curves of real short GRBs. We therefore considered a sample of short GRBs observed by Swift/XRT with data sufficiently sampled to allow fitting of the unabsorbed X-ray light curve in the 0.3–10 keV energy band using a (multiple broken) power-law model. The decay index during the deceleration phase is then identified as the slope of the final power-law segment. This choice is made to exclude the initial steep decay and plateau phase for consistency with our model (see Section 3), which considers only standard temporal decays produced by the jet deceleration in interactions with the circumburst medium.

The resulting distribution is shown in Figure 13: the mean value is 1.45 (median 1.37) and the standard deviation is 0.48.

The scatter plots for the inferred luminosities at 11 h in X-ray and VHE energy range (see Section 3.3 of the main text for their derivation) are shown in Figure 14, together with their distributions.

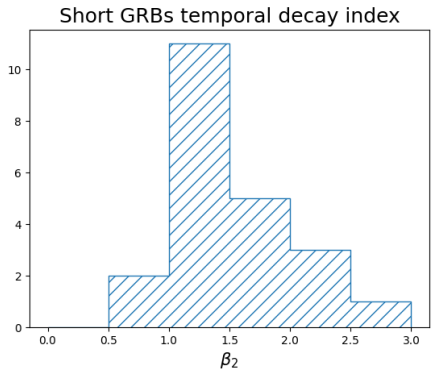


**Figure 13.** Distribution of the temporal decay indices $\beta_2$ ($F \propto t^{-\beta_2}$) of the X-ray afterglow of short GRBs. The temporal decay is obtained from a (multiple broken) power-law fit to the Swift/XRT unabsorbed light curve in the energy range 0.3–10 keV (observer frame).

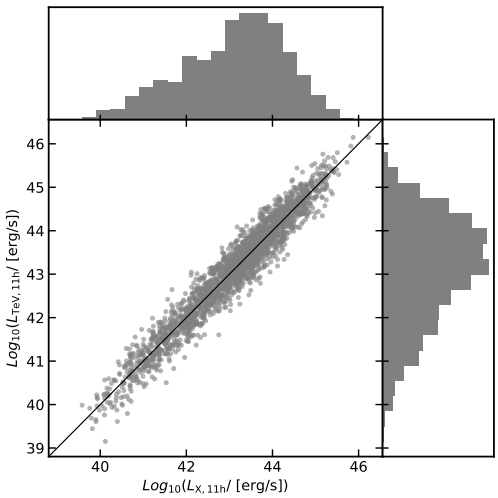


**Figure 14.** X-ray (0.3–10 keV) and VHE (0.3–1 TeV) simulated luminosities at 11 hr.

## ORCID iDs

S. Abe https://orcid.org/0000-0001-7250-3596
J. Abhir https://orcid.org/0000-0001-8215-4377
A. Abhishek https://orcid.org/0009-0005-5239-7905
F. Acero https://orcid.org/0000-0002-6606-2816
A. Acharyya https://orcid.org/0000-0002-2028-9230
R. Adam https://orcid.org/0009-0000-5380-1109
A. Aguasca-Cabot https://orcid.org/0000-0001-8816-4920
I. Agudo https://orcid.org/0000-0002-3777-6182
I. Albanese https://orcid.org/0009-0006-6223-5018
C. Alispach https://orcid.org/0000-0002-3791-1997
R. Alves Batista https://orcid.org/0000-0003-2656-064X
G. Ambrosi https://orcid.org/0000-0001-6977-9559
D. Ambrosino https://orcid.org/0009-0005-6578-893X
F. Ambrosino https://orcid.org/0000-0001-7915-996X
L. Angel https://orcid.org/0000-0003-3684-6553
C. Arcaro https://orcid.org/0000-0002-1998-9707
C. Arena https://orcid.org/0000-0002-0319-8791
T. T. H. Arnesen https://orcid.org/0009-0004-0816-0700
K. Asano https://orcid.org/0000-0001-9064-160X
H. Ashkar https://orcid.org/0000-0002-2153-1818
C. Bakshi https://orcid.org/0009-0007-1843-5386
C. Balazs https://orcid.org/0000-0001-7154-1726
M. Balbo https://orcid.org/0000-0002-6556-3344
A. Baquero Larriva https://orcid.org/0000-0002-1757-5826
V. Barbosa Martins https://orcid.org/0000-0002-5085-8828
J. A. Barrio https://orcid.org/0000-0002-0965-0259
C. Bartolini https://orcid.org/0000-0001-7233-9546
I. Batković https://orcid.org/0000-0002-1209-2542
R. Batzofin https://orcid.org/0000-0002-5797-3386
N. Bavdaz https://orcid.org/0009-0000-8954-2057
J. Becerra González https://orcid.org/0000-0002-6729-9022
G. Beck https://orcid.org/0000-0003-4916-4914
W. Benbow https://orcid.org/0000-0003-2098-170X
E. Bernardini https://orcid.org/0000-0003-3108-1141
M. G. Bernardini https://orcid.org/0000-0001-6106-3046
J. Bernete https://orcid.org/0000-0002-8108-7552
A. Berti https://orcid.org/0000-0003-0396-4190
B. Bertucci https://orcid.org/0000-0001-7584-293X
V. Beshley https://orcid.org/0000-0002-2688-0224
P. Bhattacharjee https://orcid.org/0000-0002-0258-3831
S. Bhattacharyya https://orcid.org/0000-0002-6569-5953
C. Bigongiari https://orcid.org/0000-0003-3293-8522
A. Biland https://orcid.org/0000-0002-1288-833X
E. Bissaldi https://orcid.org/0000-0001-9935-8106
M. Blaña https://orcid.org/0000-0003-2139-0944
O. Blanch https://orcid.org/0000-0002-8380-1633
J. Blazek https://orcid.org/0000-0002-5870-8947
C. Boisson https://orcid.org/0000-0001-5893-1797
G. Bonnoli https://orcid.org/0000-0003-2464-9077
Z. Bosnjak https://orcid.org/0000-0001-6536-0320
E. Bottacini https://orcid.org/0000-0001-9579-0487
M. Böttcher https://orcid.org/0000-0002-8434-5692
E. Bronzini https://orcid.org/0000-0001-8378-4303
G. Brunelli https://orcid.org/0009-0008-2078-2456
J. Buces Sáez https://orcid.org/0009-0006-8913-126X
T. Bulik https://orcid.org/0000-0003-2045-4803
A. Campoy-Ordaz https://orcid.org/0000-0001-9352-8936
B. K. Cantlay https://orcid.org/0009-0002-8750-6401
G. Capasso https://orcid.org/0000-0002-4472-4858
A. Caproni https://orcid.org/0000-0001-9707-3895
R. Capuzzo-Dolcetta https://orcid.org/0000-0002-6871-9519
S. Caroff https://orcid.org/0000-0002-1103-130X
E. Carquin https://orcid.org/0000-0002-7863-1166
E. Cascone https://orcid.org/0000-0002-7425-7517
F. Cassol https://orcid.org/0000-0002-0372-1992
G. Castignani https://orcid.org/0000-0001-6831-0687
F. Catalani https://orcid.org/0000-0001-9332-1476
D. Cerasole https://orcid.org/0000-0003-2033-756X
M. Cerruti https://orcid.org/0000-0001-7891-699X
A. Cerviño Cortínez https://orcid.org/0009-0007-1566-9507
P. M. Chadwick https://orcid.org/0000-0002-1468-2685
S. Chaty https://orcid.org/0000-0002-5769-8601
A. W. Chen https://orcid.org/0000-0001-6425-5692
Y. Chen https://orcid.org/0009-0001-5719-936X
M. Chernyakova https://orcid.org/0000-0002-9735-3608
A. Chiavassa https://orcid.org/0000-0001-6183-2589
G. Chon https://orcid.org/0000-0002-1032-1970
J. Chudoba https://orcid.org/0000-0002-6425-2579
L. Chytka https://orcid.org/0000-0001-5741-259X

G. M. Cicciari https://orcid.org/0009-0007-3885-051X
A. Cifuentes Santos https://orcid.org/0000-0003-1033-5296
C. H. Coimbra Araujo https://orcid.org/0000-0003-3588-2587
J. L. Contreras https://orcid.org/0000-0001-7282-2394
B. Cornejo https://orcid.org/0009-0003-0039-0483
J. Cortina https://orcid.org/0000-0003-4576-0452
A. Costa https://orcid.org/0000-0003-0344-8911
G. Cotter https://orcid.org/0000-0002-9975-1829
O. Cuevas https://orcid.org/0009-0004-8037-2847
Z. Curtis-Ginsberg https://orcid.org/0000-0002-0194-7576
A. D'Aì https://orcid.org/0000-0002-5042-1036
G. D'Amico https://orcid.org/0000-0001-6472-8381
P. D'Avanzo https://orcid.org/0000-0001-7164-1508
P. Da Vela https://orcid.org/0000-0003-0604-4517
L. David https://orcid.org/0000-0003-2341-9261
F. Dazzi https://orcid.org/0000-0001-5409-6544
M. de Bony de Lavergne https://orcid.org/0000-0002-4650-1666
V. De Caprio https://orcid.org/0000-0002-4587-8963
E. M. de Gouveia Dal Pino https://orcid.org/0000-0001-8058-4752
B. De Lotto https://orcid.org/0000-0003-3624-4480
M. de Naurois https://orcid.org/0000-0002-7245-201X
V. de Souza https://orcid.org/0000-0003-0865-233X
L. del Peral https://orcid.org/0000-0003-2580-5668
C. Delgado https://orcid.org/0000-0002-7014-4101
D. della Volpe https://orcid.org/0000-0001-8530-7447
D. Depaoli https://orcid.org/0000-0002-2672-4141
L. Di Bella https://orcid.org/0009-0001-4748-8360
T. Di Girolamo https://orcid.org/0000-0003-2339-4471
F. Di Pierro https://orcid.org/0000-0003-4861-432X
R. Di Tria https://orcid.org/0009-0007-1088-5307
L. Di Venere https://orcid.org/0000-0003-0703-824X
A. Dinesh https://orcid.org/0000-0002-3729-9048
E. Do Souto Espiñeira https://orcid.org/0000-0001-6974-2676
D. Dominis Prester https://orcid.org/0000-0002-9880-5039
A. Donini https://orcid.org/0000-0002-3066-724X
D. Dorner https://orcid.org/0000-0001-8823-479X
J. Dörner https://orcid.org/0000-0001-6692-6293
M. Doro https://orcid.org/0000-0001-9104-3214
L. Ducci https://orcid.org/0000-0002-9989-538X
V. V. Dwarkadas https://orcid.org/0000-0002-4661-7001
J. Ebr https://orcid.org/0000-0001-8807-6162
C. Eckner https://orcid.org/0000-0002-5135-2909
K. Egberts https://orcid.org/0009-0000-5511-7060
D. Elsässer https://orcid.org/0000-0001-6796-3205
G. Emery https://orcid.org/0000-0001-6155-4742
C. Escañuela Nieves https://orcid.org/0000-0002-7297-8126
P. Escarate https://orcid.org/0000-0002-6751-3842
M. Escobar Godoy https://orcid.org/0009-0005-7024-1330
J. Escudero Pedrosa https://orcid.org/0000-0002-4131-655X
P. Esposito https://orcid.org/0000-0003-4849-5092
D. Falceta-Goncalves https://orcid.org/0000-0002-1914-6654
E. Fedorova https://orcid.org/0000-0002-8882-7496
S. Fegan https://orcid.org/0000-0002-9978-2510
K. Feijen https://orcid.org/0000-0003-1476-3714
Q. Feng https://orcid.org/0000-0001-6674-4238
G. Ferrand https://orcid.org/0000-0002-4231-8717
M. Filipovic https://orcid.org/0000-0002-4990-9288
V. Fioretti https://orcid.org/0000-0002-6082-5384
L. Foffano https://orcid.org/0000-0002-0709-9707
G. Fontaine https://orcid.org/0000-0002-6443-5025
F. Frías García-Lago https://orcid.org/0009-0004-5848-8763
Y. Fukui https://orcid.org/0000-0002-8966-9856
G. Galanti https://orcid.org/0000-0001-7254-3029
G. Galaz https://orcid.org/0000-0002-8835-0739
S. Gallozzi https://orcid.org/0000-0003-4456-9875
V. Gammaldi https://orcid.org/0000-0003-1826-6117
S. García Soto https://orcid.org/0009-0003-9726-5901
C. Gasbarra https://orcid.org/0000-0001-8335-9614
D. Gasparrini https://orcid.org/0000-0002-5064-9495
M. Gaug https://orcid.org/0000-0001-8442-7877
J. G. Giesbrecht Formiga Paiva https://orcid.org/0000-0002-5817-2062
N. Giglietto https://orcid.org/0000-0002-9021-2888
F. Giordano https://orcid.org/0000-0002-8651-2394
M. Giroletti https://orcid.org/0000-0002-8657-8852
R. Giuffrida https://orcid.org/0000-0002-2774-3491
P. Goldoni https://orcid.org/0000-0001-5638-5817
J. M. González https://orcid.org/0000-0002-2413-0681
J. Goulart Coelho https://orcid.org/0000-0001-9386-1042
T. Gradetzke https://orcid.org/0000-0003-0646-2495
J. Granot https://orcid.org/0000-0001-8530-8941
R. Grau https://orcid.org/0000-0002-1891-6290
D. Green https://orcid.org/0000-0003-0768-2203
J. G. Green https://orcid.org/0000-0002-1130-6692
J. Grube https://orcid.org/0009-0000-9518-2326
J. Hackfeld https://orcid.org/0000-0002-1003-6408
D. Hadasch https://orcid.org/0000-0001-8663-6461
A. Hahn https://orcid.org/0000-0003-0827-5642
P. Hamal https://orcid.org/0000-0003-3139-7234
W. Hanlon https://orcid.org/0000-0002-0109-4737
S. Hara https://orcid.org/0009-0001-1220-7717
V. M. Harvey https://orcid.org/0000-0001-9090-8415
T. Hassan https://orcid.org/0000-0002-4758-9196
K. Hayashi https://orcid.org/0000-0002-8758-8139
B. Hess https://orcid.org/0009-0004-9999-171X
L. Heckmann https://orcid.org/0000-0002-6653-8407
B. Hnatyk https://orcid.org/0000-0001-7113-4709
R. Hnatyk https://orcid.org/0000-0002-6378-7678
D. Horan https://orcid.org/0000-0001-5574-2579
P. Horvath https://orcid.org/0000-0002-6710-5339
D. Hrupec https://orcid.org/0000-0002-7027-5021
S. Hussain https://orcid.org/0000-0002-0458-0490
M. Iarlori https://orcid.org/0009-0003-5838-975X
T. Inada https://orcid.org/0000-0002-6923-9314
F. Incardona https://orcid.org/0000-0002-2568-0917
S. Inoue https://orcid.org/0000-0003-1096-9424
F. Iocco https://orcid.org/0000-0002-4237-0005
A. Iuliano https://orcid.org/0000-0001-6087-9633
Jahanvi https://orcid.org/0000-0002-7217-0821
M. Jamrozy https://orcid.org/0000-0002-0870-7778
P. Janecek https://orcid.org/0000-0003-3501-7163
I. Jaroschewski https://orcid.org/0000-0001-5180-2845
P. Jean https://orcid.org/0000-0002-1757-9560
V. Jilek https://orcid.org/0000-0001-5774-7285

I. Jiménez Martínez https://orcid.org/0000-0003-2150-6919
J. Jimenez Quiles https://orcid.org/0009-0005-6729-5709
W. Jin https://orcid.org/0000-0002-1089-1754
E. Joshi https://orcid.org/0000-0001-8557-1141
J. Jurysek https://orcid.org/0000-0002-3130-4168
V. Karas https://orcid.org/0000-0002-5760-0459
H. Katagiri https://orcid.org/0000-0003-2347-8819
T. Keita https://orcid.org/0009-0006-6346-4920
D. Kerszberg https://orcid.org/0000-0002-5289-1509
M. Kherlakian https://orcid.org/0000-0003-4686-0922
D. B. Kieda https://orcid.org/0000-0003-4785-0101
R. Kissmann https://orcid.org/0000-0001-7818-0353
T. Kleiner https://orcid.org/0000-0002-4260-9186
Y. Kobayashi https://orcid.org/0009-0005-5680-6614
K. Kohri https://orcid.org/0000-0003-3764-8612
D. Kolar https://orcid.org/0009-0005-3624-9312
N. Komin https://orcid.org/0000-0003-3280-0582
A. Kong https://orcid.org/0000-0002-5105-344X
K. Kosack https://orcid.org/0000-0001-8424-3621
G. Kowal https://orcid.org/0000-0002-0176-9909
H. Kubo https://orcid.org/0000-0001-9159-9853
J. Kushida https://orcid.org/0000-0002-8002-8585
A. La Barbera https://orcid.org/0000-0002-5880-8913
N. La Palombara https://orcid.org/0000-0001-7015-6359
B. Lacave https://orcid.org/0009-0000-0601-6204
M. Láinez https://orcid.org/0000-0003-3848-922X
A. Lamastra https://orcid.org/0000-0003-2403-913X
J. Lapington https://orcid.org/0000-0003-3451-5275
S. Lazarević https://orcid.org/0000-0001-6109-8548
J.-P. Lenain https://orcid.org/0000-0001-7284-9220
F. Leone https://orcid.org/0000-0001-7626-3788
E. Leonora https://orcid.org/0000-0002-0536-3551
G. Leto https://orcid.org/0000-0002-0040-5011
S. Lombardi https://orcid.org/0000-0002-6336-865X
F. Longo https://orcid.org/0000-0003-2501-2270
M. López-Moya https://orcid.org/0000-0002-8791-7908
A. López-Oramas https://orcid.org/0000-0003-4603-1884
J. Lozano Bahilo https://orcid.org/0000-0003-0613-140X
P. L. Luque-Escamilla https://orcid.org/0000-0002-3306-9456
O. Macias https://orcid.org/0000-0001-8867-2693
M. Makariev https://orcid.org/0000-0002-1622-3116
S. Mangano https://orcid.org/0000-0001-5872-1191
A. Marchetti https://orcid.org/0009-0000-1579-9108
M. Mariotti https://orcid.org/0000-0003-3297-4128
S. Markoff https://orcid.org/0000-0001-9564-0876
I. Márquez https://orcid.org/0000-0003-2629-1945
G. Marsella https://orcid.org/0000-0002-3152-8874
J. Martí https://orcid.org/0000-0001-5302-0660
D. Martín Domínguez https://orcid.org/0009-0006-8054-8704
M. Martínez https://orcid.org/0000-0002-9763-9155
O. Martinez https://orcid.org/0000-0002-3353-7707
S. Menon https://orcid.org/0009-0007-6360-6500
E. Mestre https://orcid.org/0000-0003-3968-1782
D. M.-A. Meyer https://orcid.org/0000-0001-8258-9813
D. Miceli https://orcid.org/0000-0002-2686-0098
M. Miceli https://orcid.org/0000-0003-0876-8391
M. Michailidis https://orcid.org/0009-0008-3653-1109
T. Miener https://orcid.org/0000-0003-1821-7964
J. M. Miranda https://orcid.org/0000-0002-1472-9690
R. Moderski https://orcid.org/0000-0002-8663-3882
M. Molero https://orcid.org/0000-0003-0967-715X
C. Molfese https://orcid.org/0000-0002-2756-9075
E. Molina https://orcid.org/0000-0003-1204-5516
K. Morik https://orcid.org/0000-0003-1153-5986
A. Morselli https://orcid.org/0000-0002-7704-9553
E. Moulin https://orcid.org/0000-0003-4007-0145
A. L. Müller https://orcid.org/0000-0002-8473-695X
T. Murach https://orcid.org/0000-0003-1128-5008
H. Muraishi https://orcid.org/0000-0003-3054-5725
L. Nava https://orcid.org/0000-0001-5960-0455
R. Nemmen https://orcid.org/0000-0003-3956-0331
J. Niemiec https://orcid.org/0000-0001-6036-8569
D. Nieto https://orcid.org/0000-0003-3343-0755
M. Nievas Rosillo https://orcid.org/0000-0002-8321-9168
M. Nikołajuk https://orcid.org/0000-0003-4075-6745
K. Noda https://orcid.org/0000-0003-1397-6478
D. Nosek https://orcid.org/0000-0001-6219-200X
V. Novotny https://orcid.org/0000-0002-4319-4541
S. Nozaki https://orcid.org/0000-0002-6246-2767
R. A. Ong https://orcid.org/0000-0002-4837-5253
M. Orlandini https://orcid.org/0000-0003-0946-3151
S. Orlando https://orcid.org/0000-0003-2836-540X
J. Otero-Santos https://orcid.org/0000-0002-4241-5875
I. Oya https://orcid.org/0000-0002-3881-9324
M. Ozlati Moghadam https://orcid.org/0009-0003-2479-1863
A. Pagliaro https://orcid.org/0000-0002-6841-1362
A. Pandey https://orcid.org/0000-0003-3820-0887
G. Panebianco https://orcid.org/0000-0002-3410-8613
D. Paneque https://orcid.org/0000-0002-2830-0502
F. R. Pantaleo https://orcid.org/0000-0002-0144-5373
J. M. Paredes https://orcid.org/0000-0002-1566-9044
A. Pe'er https://orcid.org/0000-0001-8667-0889
M. Pech https://orcid.org/0000-0002-8421-0456
M. Pecimotika https://orcid.org/0000-0002-4699-1845
M. Peresano https://orcid.org/0000-0002-7537-7334
J. Pérez-Romero https://orcid.org/0000-0002-9408-3120
M. Persic https://orcid.org/0000-0003-1853-4900
O. Petruk https://orcid.org/0000-0003-3487-0349
F. Pfeifle https://orcid.org/0009-0009-4785-6643
E. Pietropaolo https://orcid.org/0000-0002-6633-9846
M. Pihet https://orcid.org/0009-0000-4691-3866
L. Pinchbeck https://orcid.org/0009-0009-6802-2461
F. Pintore https://orcid.org/0000-0002-3869-2925
C. Pittori https://orcid.org/0000-0001-6661-9779
F. Podobnik https://orcid.org/0000-0001-6125-9487
G. Ponti https://orcid.org/0000-0003-0293-3608
E. Prandini https://orcid.org/0000-0003-4502-9053
G. Principe https://orcid.org/0000-0003-0406-7387
M. Prouza https://orcid.org/0000-0002-3238-9597
G. Pühlhofer https://orcid.org/0000-0003-4632-4644
M. Punch https://orcid.org/0000-0002-4710-2165
S. Rainò https://orcid.org/0000-0002-9181-0345
R. Rando https://orcid.org/0000-0001-6992-818X
S. Recchia https://orcid.org/0000-0002-1858-2622
A. Reimer https://orcid.org/0000-0001-8604-7077
O. Reimer https://orcid.org/0000-0001-6953-1385
I. Reis https://orcid.org/0000-0002-0771-3332
A. Reisenegger https://orcid.org/0000-0003-4059-6796
W. Rhode https://orcid.org/0000-0003-2636-5000
M. Ribó https://orcid.org/0000-0002-9931-4557

C. Ricci https://orcid.org/0000-0001-5231-2645
J. Rico https://orcid.org/0000-0003-4137-1134
L. Riitano https://orcid.org/0000-0003-2875-3066
V. Rizi https://orcid.org/0000-0002-5277-6527
G. Rodriguez Fernandez https://orcid.org/0000-0002-4683-230X
P. Romano https://orcid.org/0000-0003-0258-7469
G. Romeo https://orcid.org/0000-0003-3239-6057
J. Rosado https://orcid.org/0000-0001-8208-9480
A. Rosales de Leon https://orcid.org/0000-0002-5815-8447
I. Sadeh https://orcid.org/0000-0003-1387-8915
L. Saha https://orcid.org/0000-0002-3171-5039
T. Saito https://orcid.org/0000-0001-6201-3761
M. Sánchez-Conde https://orcid.org/0000-0002-3849-9164
P. Sangiorgi https://orcid.org/0000-0001-8138-9289
H. Sano https://orcid.org/0000-0003-2062-5692
R. Santos-Lima https://orcid.org/0000-0001-6880-4468
V. Sapienza https://orcid.org/0000-0002-6045-136X
S. Sarkar https://orcid.org/0000-0002-3542-858X
F. G. Saturni https://orcid.org/0000-0002-1946-7706
F. Schiavone https://orcid.org/0009-0003-5919-3329
P. Schipani https://orcid.org/0000-0003-0197-589X
F. Schussler https://orcid.org/0000-0003-1500-6571
M. Seglar Arroyo https://orcid.org/0000-0001-8654-409X
O. Sergijenko https://orcid.org/0000-0002-9212-7118
H. Siejkowski https://orcid.org/0000-0003-1673-2145
A. Simongini https://orcid.org/0009-0000-3416-9865
V. Sliusar https://orcid.org/0000-0002-4387-9372
A. Slowikowska https://orcid.org/0000-0003-4525-3178
I. Sofia https://orcid.org/0009-0009-2451-3138
A. Stamerra https://orcid.org/0000-0002-9430-5264
S. Stanič https://orcid.org/0000-0003-3344-8381
T. Starecki https://orcid.org/0000-0002-4730-6803
R. Starling https://orcid.org/0000-0001-5803-2038
T. Stolarczyk https://orcid.org/0000-0002-0551-7581
Y. Suda https://orcid.org/0000-0002-2692-5891
A. Sunny https://orcid.org/0009-0002-2493-8987
R. Takeishi https://orcid.org/0000-0001-6335-5317
S. J. Tanaka https://orcid.org/0000-0002-8796-1992
F. Tavecchio https://orcid.org/0000-0003-0256-0995
Y. Terada https://orcid.org/0000-0002-2359-1857
V. Testa https://orcid.org/0000-0003-1033-1340
Y. Tian https://orcid.org/0009-0005-7165-3791
L. Tibaldo https://orcid.org/0000-0001-7523-570X
S. J. Tingay https://orcid.org/0000-0002-8195-7562
C. J. Todero Peixoto https://orcid.org/0000-0003-3669-8212
F. Tombesi https://orcid.org/0000-0002-6562-8654
D. Tonev https://orcid.org/0000-0003-4431-6157
F. Torradeflot https://orcid.org/0000-0003-1160-1517
D. F. Torres https://orcid.org/0000-0002-1522-9065
N. Tothill https://orcid.org/0000-0002-9931-5162
G. Tovmassian https://orcid.org/0000-0002-2953-7528
A. Trois https://orcid.org/0000-0002-3180-6002
A. Tsiahina https://orcid.org/0009-0006-6205-8728
A. Tutone https://orcid.org/0000-0002-2840-0001
L. Vaclavek https://orcid.org/0000-0002-0910-3415
M. Vacula https://orcid.org/0000-0003-4844-3962
C. van Eldik https://orcid.org/0000-0001-9669-645X
J. Vandenbroucke https://orcid.org/0000-0002-9867-6548
M. Vázquez Acosta https://orcid.org/0000-0002-2409-9792
S. Vercellone https://orcid.org/0000-0003-1163-1396
S. D. Vergani https://orcid.org/0000-0001-9398-4907
I. Viale https://orcid.org/0000-0001-5031-5930
A. Vigliano https://orcid.org/0009-0001-3508-4019
J. Vignatti https://orcid.org/0000-0002-1494-9562
C. F. Vigorito https://orcid.org/0000-0002-0069-9195
E. Visentin https://orcid.org/0009-0009-3200-1087
V. Voitsekhovskyi https://orcid.org/0000-0002-3906-4840
S. Vorobiov https://orcid.org/0000-0001-8679-3424
I. Vovk https://orcid.org/0000-0003-3444-3830
T. Vuillaume https://orcid.org/0000-0002-5686-2078
R. Walter https://orcid.org/0000-0003-2362-4433
M. Wechakama https://orcid.org/0000-0001-8279-4550
A. Wierzcholska https://orcid.org/0000-0003-4472-7204
M. Will https://orcid.org/0000-0002-7504-2083
F. Wohlleben https://orcid.org/0000-0002-6451-4188
A. Wolter https://orcid.org/0000-0001-5840-9835
T. Yamamoto https://orcid.org/0000-0001-9734-8203
R. Yamazaki https://orcid.org/0000-0002-1251-7889
T. Yoshikoshi https://orcid.org/0000-0002-6045-9839
M. Zacharias https://orcid.org/0000-0001-5801-3945
R. Zanmar Sanchez https://orcid.org/0000-0002-6997-0887
D. Zavrtanik https://orcid.org/0000-0002-4596-1521
A. Zech https://orcid.org/0000-0002-4388-5625
V. I. Zhdanov https://orcid.org/0000-0003-3690-483X
M. Živec https://orcid.org/0009-0003-8528-1453
J. Zuriaga-Puig https://orcid.org/0000-0003-0652-6700
A. Colombo https://orcid.org/0000-0002-7439-4773

## References

Abbott, B. P., Abbott, R., Abbott, T. D., et al. 2017a, PhRvL, 119, 161101
Abbott, B. P., Abbott, R., Abbott, T. D., et al. 2017b, ApJL, 848, L12
Abbott, B. P., Abbott, R., Abbott, T. D., et al. 2020, LRR, 23, 3
Abbott, R., Abbott, T. D., Acernese, F., et al. 2023, PhRvX, 13, 011048
Abdalla, H., Abramowski, A., Aharonian, F., et al. 2017, ApJL, 850, L22
Abdalla, H., Adam, R., Aharonian, F., et al. 2019, Natur, 575, 464
Abdalla, H., Adam, R., Aharonian, F., et al. 2020, ApJL, 894, L16
Abe, H., Abe, S., Acciari, V. A., et al. 2024, MNRAS, 527, 5856
Abe, K., Abe, S., Abhishek, A., et al. 2025a, ApJL, 988, L42
Abe, S., Abhir, J., Abhishek, A., et al. 2025b, A&A, 700, A96
Acciari, V. A., Ansoldi, S., Antonelli, L. A., et al. 2021, ApJ, 908, 90
Acernese, F., Agathos, M., Agatsuma, K., et al. 2015, CQGra, 32, 024001
Acharya, B. S., Actis, M., Aghajani, T., et al. 2013, APh, 43, 3
Adams, T., Buskulic, D., Germain, V., et al. 2016, CQGra, 33, 175012
Aharonian, F., Akhperjanian, A. G., Barres de Almeida, U., et al. 2009, A&A, 495, 505
Akutsu, T., Ando, M., Arai, K., et al. 2019, CQGra, 36, 165008
Albert, A., Alfaro, R., Alvarez, C., et al. 2022, ApJ, 936, 126
Ashkar, H., Brun, F., Füßling, M., et al. 2021, JCAP, 03, 045
Astropy Collaboration, Robitaille, T. P., Tollerud, E. J., et al. 2013, A&A, 558, A33
Astropy Collaboration, Price-Whelan, A. M., Sipőcz, B. M., et al. 2018, AJ, 156, 123
Astropy Collaboration, Price-Whelan, A. M., Lim, P. L., et al. 2022, ApJ, 935, 167
Banerjee, B., Oganesyan, G., Branchesi, M., et al. 2023, A&A, 678, A126
Bartos, I., Corley, K. R., Gupte, N., et al. 2019, MNRAS, 490, 3476
Bartos, I., Veres, P., Nieto, D., et al. 2014, MNRAS, 443, 738
Bartos, I., Di Girolamo, T., Gair, J. R., et al. 2018, MNRAS, 477, 639
Berger, E. 2014, ARA&A, 52, 43
Blanch, O., Gaug, M., Noda, K., et al. 2020, GCN, 28659, 1
Blandford, R. D., & McKee, C. F. 1976, PhFl, 19, 1130
Bošnjak, Ž., Zhang, B. T., Murase, K., & Ioka, K. 2024, MNRAS, 528, 4307
Bulgarelli, A., Caroff, S., Addis, A., et al. 2022, ICRC, 37, 937
Burgay, M., D'Amico, N., Possenti, A., et al. 2003, Natur, 426, 531
Cannon, K., Cariou, R., Chapman, A., et al. 2012, ApJ, 748, 136
Cao, Z., Aharonian, F., An, Q., et al. 2023, SciA, 9, eadj2778

Cherenkov Telescope Array Consortium, Acharya, B. S., Agudo, I., et al. 2019, Science with the Cherenkov Telescope Array (World Scientific)
Cherenkov Telescope Array ObservatoryCherenkov Telescope Array Consortium 2021, CTAO Instrument Response Functions, Version prod5-v0.1, Zenodo, doi:10.5281/zenodo.5499840
Colombo, A., Salafia, O. S., Gabrielli, F., et al. 2022, ApJ, 937, 79
Colombo, A., Sharan Salafia, O., Ghirlanda, G., et al. 2025, A&A, 704, A260
Dal Canton, T., Nitz, A. H., Lundgren, A. P., et al. 2014, PhRvD, 90, 082004
Dálya, G., Díaz, R., Bouchet, F. R., et al. 2022, MNRAS, 514, 1403
D'Avanzo, P., Salvaterra, R., Sbarufatti, B., et al. 2012, MNRAS, 425, 506
Dey, A., Schlegel, D. J., Lang, D., et al. 2019, AJ, 157, 168
Donath, A., Terrier, R., Remy, Q., et al. 2023, A&A, 678, A157
Egberts, K., Hoischen, C., Steppa, C., et al. 2022, SPIE, 12186, 121860L
Fong, W., Berger, E., Margutti, R., & Zauderer, B. A. 2015, ApJ, 815, 102
Franceschini, A., & Rodighiero, G. 2017, A&A, 603, A34
Funk, S., Hinton, J. A. & CTA Consortium 2013, APh, 43, 348
Ghirlanda, G., Ghisellini, G., & Nava, L. 2011, MNRAS, 418, L109
Ghirlanda, G., Salafia, O. S., Pescalli, A., et al. 2016, A&A, 594, A84
Ghirlanda, G., Salafia, O. S., Paragi, Z., et al. 2019, Sci, 363, 968
Goldstein, A., Veres, P., Burns, E., et al. 2017, ApJL, 848, L14
Green, J. G., Patricelli, B., Stamerra, A., & Seglar-Arroyo, M. 2026, arXiv:2602.06783
H. E. S. S. Collaboration, Abdalla, H., Aharonian, F., et al. 2021, Sci, 372, 1081
Hope, J. P., van Eerten, H. J., Kundu, S., & Schady, P. 2025, MNRAS, 538, 281
Kaneko, Y., Ramirez-Ruiz, E., Granot, J., et al. 2007, ApJ, 654, 385
Kathirgamaraju, A., Barniol Duran, R., & Giannios, D. 2018, MNRAS, 473, L121
Kiendrebeogo, R. W., Farah, A. M., Foley, E. M., et al. 2023, ApJ, 958, 158
Kumar, P., & Granot, J. 2003, ApJ, 591, 1075
Kuralkar, H. J., Sah, M. R., & Mukherjee, S. 2025, arXiv:2507.18955
Lamb, G. P., & Kobayashi, S. 2017, MNRAS, 472, 4953
Levan, A. J., Gompertz, B. P., Salafia, O. S., et al. 2024, Natur, 626, 737
LHAASO Collaboration, Cao, Z., Aharonian, F., et al. 2023, Sci, 380, 1390
Ligo Scientific Collaboration, VIRGO Collaboration, & Kagra Collaboration 2025a, GCN, 38991, 1
Ligo Scientific Collaboration, VIRGO Collaboration, & Kagra Collaboration 2025b, GCN, 38043, 1
LIGO Scientific Collaboration, Aasi, J., Abbott, B. P., et al. 2015, CQGra, 32, 074001
MAGIC Collaboration, Acciari, V. A., Ansoldi, S., et al. 2019a, Natur, 575, 455
MAGIC Collaboration, Acciari, V. A., Ansoldi, S., et al. 2019b, Natur, 575, 459
Margutti, R., Zaninoni, E., Bernardini, M. G., et al. 2013, MNRAS, 428, 729
Messick, C., Blackburn, K., Brady, P., et al. 2017, PhRvD, 95, 042001
Miceli, D., & Nava, L. 2022, Galax, 10, 66
Mondal, T., Chakraborty, S., Resmi, L., & Bose, D. 2025, ApJ, 983, 35
Nava, L. 2021, Univ, 7, 503
Nitz, A. H., Dent, T., Dal Canton, T., Fairhurst, S., & Brown, D. A. 2017, ApJ, 849, 118
O'Reilly, B., Branchesi, M., Haino, S., & Gemme, G. 2020, Noise Curves Used for Simulations in the Update of the Observing Scenarios Paper, LIGO-T2000012-v1, https://dcc.ligo.org/LIGO-T2000012/public
Oya, I., Aubert, P., Baroncelli, L., et al. 2024, SPIE, 13101, 537
Özel, F., & Freire, P. 2016, ARA&A, 54, 401
Paneque, D., Teshima, M., Seglar Arroyo, M., et al. 2024, GCN, 38443, 1
Patricelli, B., Stamerra, A., Razzano, M., Pian, E., & Cella, G. 2018, JCAP, 05, 056
Pellouin, C., & Daigne, F. 2024, A&A, 690, A281
Petrov, P., Singer, L. P., Coughlin, M. W., et al. 2022, ApJ, 924, 54
Planck Collaboration, Ade, P. A. R., Aghanim, N., et al. 2016, A&A, 594, A13
Rastinejad, J. C., Gompertz, B. P., Levan, A. J., et al. 2022, Natur, 612, 223
Rouco Escorial, A., Fong, W., Berger, E., et al. 2023, ApJ, 959, 13
Ryan, G., van Eerten, H., Piro, L., & Troja, E. 2020, ApJ, 896, 166
Salafia, O. S. 2025, A&A, 702, A54
Salafia, O. S., Berti, A., Covino, S., et al. 2022b, ICRC, 37, 944
Salafia, O. S., Colombo, A., Gabrielli, F., & Mandel, I. 2022a, A&A, 666, A174
Salafia, O. S., & Ghirlanda, G. 2022, Galax, 10, 93
Salafia, O. S., Ghirlanda, G., Ascenzi, S., & Ghisellini, G. 2019, A&A, 628, A18
Salafia, O. S., & Giacomazzo, B. 2021, A&A, 645, A93
Sarin, N., Lasky, P. D., Vivanco, F. H., et al. 2022, PhRvD, 105, 083004
Savchenko, V., Ferrigno, C., Kuulkers, E., et al. 2017, ApJL, 848, L15
Seglar-Arroyo, M., Ashkar, H., de Lavergne, M. d. B., & Schüssler, F. 2024, ApJS, 274, 1
Singer, L. 2021, Data-driven Expectations for Electromagnetic Counterpart Searches Based on LIGO/Virgo Public Alerts: O5 Simulations, v1, Zenodo, doi:10.5281/zenodo.4765752
Singer, L. P., Criswell, A. W., Leggio, S. C., et al. 2025, PASP, 137, 074501
Singer, L. P., Price, L. R., Farr, B., et al. 2014, ApJ, 795, 105
The LIGO Scientific Collaborationthe Virgo Collaborationthe KAGRA Collaboration, et al. 2025, arXiv:2508.18083
Usman, S. A., Nitz, A. H., Harry, I. W., et al. 2016, CQGra, 33, 215004
Veitch, J., Raymond, V., Farr, B., et al. 2015, PhRvD, 91, 042003
Wainstein, L. A., & Zubakov, V. D. 1962, Extraction of Signals from Noice (Prentice-Hall)
Wyatt, S. D., Tohuvavohu, A., Arcavi, I., et al. 2020, ApJ, 894, 127
Yuan, C., Murase, K., Guetta, D., et al. 2022, ApJ, 932, 80
Zhang, B., & Mészáros, P. 2002, ApJ, 571, 876